J. Membrane Biol. 77, 123–152 (1984)

The Journal of
Membrane Biology

Generalized Kinetic Analysis of Ion-Driven Cotransport Systems: A Unified Interpretation of Selective Ionic Effects on Michaelis Parameters

Dale Sanders*†, Ulf-Peter Hansen‡, Dietrich Gradmann§ and Clifford L. Slayman†

† Department of Physiology, Yale University School of Medicine, New Haven, Connecticut 06510,
‡ Institut für Angewandte Physik, Neue Universität, 2300 Kiel, West Germany, and
§ Max-Planck-Institut für Biochemie, 8033 Martinsried-bei-München, West Germany

Summary. A major obstacle to the understanding of gradient-driven transport systems has been their apparently wide kinetic diversity, which has seemed to require a variety of ad hoc mechanisms. Ordinary kinetic analysis, however, has been hampered by one mathematically powerful but physically dubious assumption: that rate limitation occurs in transmembrane transit, so that ligand-binding reactions are at equilibrium. Simple models lacking that assumption turn out to be highly flexible and are able to describe most of the observed kinetic diversity in co- and counter-transport systems.

Our "minimal" model of cotransport consists of a single transport loop linking six discrete states of a carrier-type molecule. The state transitions include one transmembrane charge-transport step, and one step each for binding of substrate and cosubstrate (driver ion) at each side of the membrane. The properties of this model are developed by sequential use of realistic *experimental* simplifications and generalized numerical computations, focussed to create known effects of substrate, driver ion, and membrane potential upon the apparent Michaelis parameters (J_{max}, K_m) of isotopic substrate influx.

Specific behavior of the minimal model depends upon the arrangement of magnitudes of individual reaction constants among the whole set (12) in the loop. Well defined arrangements have been found which permit either increasing membrane potential or increasing external driver-ion selectively to reduce the substrate K_m, elevate J_{max}, jointly raise both K_m and J_{max}, or lower K_m while raising J_{max}. Other arrangements allow rising internal driver ion to act like either a competitive or a noncompetitive inhibitor of entry, or allow internal substrate to shut down ("transinhibit") influx despite large inward driving forces.

These findings obviate most postulates of special mechanisms in cotransport: e.g., stoichiometry changes, ion wells, carrier-mediated leakage, and gating – *at least as explanations for existing transport kinetic data.* They also provide a simple interpretation of certain kinds of homeostatic regulation, and lead to speculation that the observed diversity in cotransport kinetics reflects control-related selection of reaction rate constants, rather than fundamental differences of mechanism.

Key Words cotransport · Michaelis constant · reaction kinetic model · rapid equilibrium kinetics · affinity/velocity models · stoichiometry change · proton well

* *Present address:* Department of Biology, University of York, Heslington, York Y01 5DD, England.

Introduction

Over the past 20 years, it has become clear that most solutes recognized as "actively" transported through biological membranes are in fact driven by coupling to the downhill movement of specific ions: sodium ions in animal cells and protons in prokaryotic cells and walled eukaryots. And the sodium ions or protons are in turn driven uphill through the same membranes by coupling to hydrolysis of ATP. The molecular devices that accomplish coupling between Na^+ or H^+ and other solutes (first postulated by Crane, Miller and Bihler (1961) and Mitchell (1963) have come to be known as cotransport systems or symports (when the "driver" ion and coupled solute move in the same direction) and countertransport systems or antiports (when the driver ion and coupled solute move in opposite directions).

Initial observations that many transport systems exhibit Michaelis-Menten kinetics led to attempts to describe carrier-mediated transport in terms analogous to enzyme kinetics (Wilbrandt & Rosenberg, 1961). Since that time, it has been customary to analyze co- and counter-transport mechanisms by asking how the levels and concentration gradients of the driver ion affect transport kinetics of the coupled substrate. An early analysis by Schultz and Curran (1970) predicted that the specific effect of the driver ion on solute flux could be sufficient to deduce binding order of the two ligands.

Experiments with a wide range of transporting membranes have revealed great kinetic heterogeneity in co- and counter-transport mechanisms. Variations of driver ion concentration can have selective effects either on the apparent Michaelis constant (K_m) for coupled solute flux (in animal cells: Curran et al., 1967; Munck &

Schultz, 1969; Aronson & Sacktor, 1975; in bacteria: Stock & Roseman, 1971; Niiya et al., 1980; in fungi: Cuppoletti & Segel, 1975*a*; in plants: Delrot & Bonnemain, 1981; Despeghel & Delrot, 1983), or on the J_{max} (in animal cells: Goldner, Schultz & Curran, 1969; Peterson & Raghupathy, 1973; Hopfer, 1977; in bacteria: Lanyi, 1978), or jointly on both K_m and J_{max} (Inui & Christensen, 1966; Eddy, Mulcahy & Thomson, 1967).

The data have spawned a variety of detailed carrier schemes, but intrinsic algebraic complexity has led, with a few exceptions (e.g., Stein, 1976; Hill, 1977), to use of one major simplifying assumption: that the carrier exists in *equilibrium* with transported ligands, making transmembrane transit rate-limiting to the overall rate of transport (Vidaver & Shepherd, 1968; Schultz & Curran, 1970; Heinz, Geck & Wilbrandt, 1972; Jacquez, 1972; van den Broek & van Steveninck, 1980; Turner, 1981). While this assumption is indeed powerful from an algebraic point of view (reducing by almost twofold the number of reaction "constants" to be manipulated), it is hindered by the absence of physical support and divergent mechanistic consequences. For example, "quasiallosteric" action of driver ions on carrier affinity for the coupled solute seems required to account for selective K_m effects (Heinz et al., 1972; Geck & Heinz, 1978); and ionic modulation of intrinsic carrier mobility has been postulated to account for J_{max} effects (Heinz et al., 1972).

Such separate modes of action of ions on coupled transport systems has seemed awkward to us and improbable in view of the close evolutionary and functional relationships between systems displaying separate K_m and J_{max} effects (*see*, for example, summary for Na^+/amino acid cotransport in Cohen, 1980). It is therefore the purpose of this paper to develop a general model, for isotopic fluxes through cotransport systems, which makes no *a priori* assumption about which reaction step in the overall transport cycle is fast, or which is rate limiting. The model also avoids all special postulates, such as those involving electric field-induced changes in microscopic ion activity, and deals only with the straightforward consequences of ordered binding and unbinding of the driver ion and coupled solute. One of our major purposes has been to examine the kinetic flexibility of the simplest models for cotransport. [Those models with the fewest steps and carrier states involve ordered binding of ligands. Therefore, we consider these models in detail rather than those involving random addition of ligands or transit of the membrane by partially-loaded carrier forms; the latter schemes are certain to be at least as flexible as the models under consideration. However, some basic properties of the kinetically more complex schemes are considered in the Discussion.] The major conclusion that emerges is that the entire observed range of kinetic relationships between driver ions and coupled solutes depends only on the relative magnitudes of individual reaction constants in the overall transport cycle. From this perspective, only minor changes – from one co- or counter-transport system to another – are required by the diverse published data. A preliminary report of these results has been presented (Sanders et al., 1982).

The Model

Outline and Assumptions

In keeping with the definitions and conventions of a previous discussion (Hansen et al., 1981), we shall treat here only Class-I cotransport models: those having a single transport loop, in which the carrier transits the membrane by one path as a charged species and transits by one other path as a neutral species. For the purpose of current-voltage analysis, all such models – regardless of the total number of reaction steps they contain – can be reduced to a two-state form, in which all voltage-independent steps are lumped together. Such extensive reduction is not possible, however, when unidirectional (isotopic) flux is to be examined as a function of the concentrations of two ligands binding at both sides of the membrane. In that case the minimal model contains six forms of the carrier, and a conventional 6-state transport cycle has been adopted for the present analysis. [The manner in which empirical reaction constants would need to be reinterpreted, should still more carrier states be identified in a particular co- or counter-transport system, can be described by means of "reserve factors" (Hansen et al., 1981), as discussed in Appendix III.]

Simple Class-I cotransport models with two ligands (H^+, S) and six states of the carrier (X) can be drawn in four different ways, depending on the order of binding and release of the driver ion and coupled substrate. These are shown in Fig. 1. If we assume a system designed for cellular *uptake* of a substrate (S), ordered binding and release of substrate relative to the driver ion can occur in one of four ways: first on-last off (Fig. 1*A*), first on-first off (Fig. 1*B*), last on-last off (Fig. 1*C*), and last on-first off (Fig. 1*D*). Use of H^+ as the driver ion is arbitrary, of course, as is assignment of charge transport to the doubly-loaded carrier (permeable carrier forms: SXH^+ and X) rather than the unloaded carrier (SXH and X^-). Neither assumption affects the fundamental kinetic relationships between transported ions and coupled substrates, although charge transport via X^- does change certain algebraic terms, in a symmetric fashion among the four reaction diagrams.

All of the diagrams in Fig. 1 can be represented by the single scheme drawn in Fig. 2*A*, in which bound ligands at the inner and outer faces of the membrane are combined into the carrier-state concentrations N_3, N_1, N_4, and N_2; and free ligand concentrations are subsumed into the unidirectional reaction constants, k_{53}, k_{31}, k_{64}, and k_{42}. Under the condition that the particular ion or substrate concentration is not changing, this compressed notation is convenient for algebraic manipulation. If it is necessary to make a concentration explicit, then the following correspondence can be defined, for example with reaction constants in the first on-last off ("*FL*") model, Fig. 1*A*: $k_{53}=k^o_{53}[S]_i$; $k_{31}=k^o_{31}[H^+]_i$; $k_{64}=k^o_{64}[S]_o$; and $k_{42}=k^o_{42}[H^+]_o$, where in each case k^o designates the true reaction constant defined without respect to ligand concentration. Explicit parameter-substrate correspondences between the generalized diagram of Fig. 2*A* and all four ordered diagrams of Fig. 1 are given in the legend to Fig. 2. The right half of the figure (*B*) transfers the subscripting nomenclature of Fig. 2*A* to the "*FL*" model of Fig. 1, and is intended as a ready reference for the presentation of results, particularly the discussions of Figs. 2–14.

The majority of co- and counter-transport systems thus far examined operate electrophoretically, transporting net positive charges inward across cell membranes. This is true for amino acids, sugars, anions [e.g., Cl^- driven with H^+ (Sanders, 1980*b*) or glutamate and H^+ (Mitchell, Booth & Hamilton, 1979)], and cations [i.e., Ca^{++} driven against Na^+ (Reeves & Sutko, 1980)]. It is essential, therefore, to incorporate the effect of the membrane electric field on the transport system. At present that must be done somewhat arbitrarily, and we have adopted as a first approach the procedure of Läuger and Stark (1970), assuming the existence of a symmetric Eyring barrier in the membrane. For the diagrams of Figs. 1 and 2, the reaction constants for the charge-transit step can then be written

$$k_{12}=k^o_{12}\exp(zu/2)$$

and

$$k_{21}=k^o_{21}\exp(-zu/2) \qquad (1a,b)$$

in which z is the net charge on the carrier during transit, u is the *reduced membrane potential*, defined as $F\Delta\psi/RT$, and the k^o's are the transit reaction constants at zero membrane potential. ($\Delta\psi$ is the measured membrane potential, taking the cell exterior to be zero; and F, R, and T have their usual meanings. The factor 2 indicates symmetry in the Eyring barrier; in a more general form of Eq. (1), this could be replaced by a separate parameter to indicate the position in the membrane of the barrier peak.) Precisely analogous equations obtain in the case (not diagrammed in Fig. 1) when crossing of the unloaded carrier is taken to be the charge-transit step:

$$k_{56}=k^o_{56}\exp(zu/2)$$

and

$$k_{65}=k^o_{65}\exp(-zu/2) \qquad (2a,b)$$

though is must be kept in mind that z itself is then negative.

Three additional properties will be assigned to the diagrams of Figs. 1 and 2: (i) All reaction steps drawn are physically discrete, and in particular the electric field through the membrane affects only the charge-transit step,

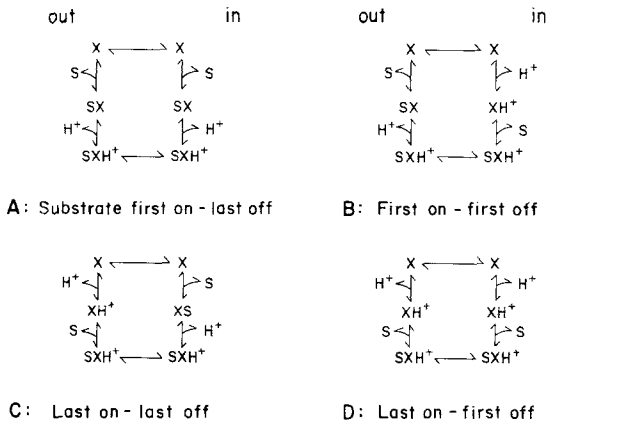

Fig. 1. The four topologically alternative models for cotransport of a solute (S) with a driver ion (H^+), mediated by a carrier (X). All models depict transport of positive charge on the loaded carrier; other cases in which the loaded carrier is neutral and the unloaded carrier negatively charged are also considered in the text. The models assume that only the unloaded and fully loaded forms of the carrier permeate the membrane

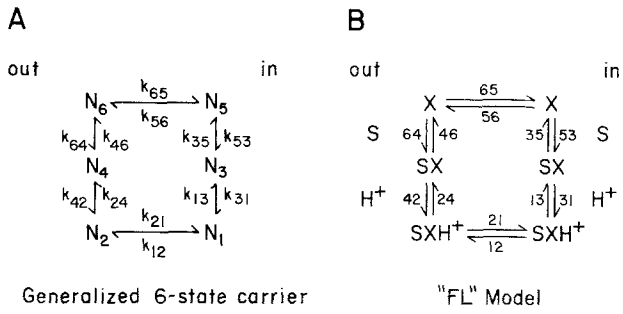

Fig. 2. The general model describing all four carriers in Fig. 1. (*A*): Reaction from carrier state N_i to state N_j is characterized by the reaction constant k_{ij}, as shown. Where appropriate, designated reaction constants subsume terms for membrane potential [*see* Eqs. (1) and (2)] or ligand concentrations. Since binding order is different for each of the four carrier models in Fig. 1, the ligand subsumed in each of the reaction constants k_{64}, k_{42}, k_{53} and k_{31} varies, and the identities are given below.

Parameter-ligand correspondence for 6-state cotransport systems

Generalized diagram	Ordered diagrams			
	"FL" (Fig. 1*A*)	"FF" (Fig. 1*B*)	"LL" (Fig. 1*C*)	"LF" (Fig. 1*D*)
k_{64}	$k^o_{64}\cdot[S]_o$	$[S]_o$	$[H^+]_o$	$[H^+]_o$
k_{42}	$k^o_{42}\cdot[H^+]_o$	$[H^+]_o$	$[S]_o$	$[S]_o$
k_{31}	$k^o_{31}\cdot[H^+]_i$	$[S]_i$	$[H^+]_i$	$[S]_i$
k_{53}	$k^o_{53}\cdot[S]_i$	$[H^+]_i$	$[S]_i$	$[H^+]_i$

(*B*): Hybrid drawing of the "FL" model (Fig. 1*A*) displaying the subscripts for reaction constants. This is given as a nomenclatural reference for *Results*, particularly to assist with the description of Figs. 3–14

not the chemical binding reactions at the membrane interfaces. This seemed, to us, the simplest assumption to make concerning the effect of $\Delta\psi$. (ii) Under any experimental condition considered, the transport system is in steady state; that is, for each state (j) of the carrier $dN_j/dt = 0$. (iii) The total concentration of carrier in the membrane is constant and can be defined as

$$N \equiv r_3 N_3 + r_1 N_1 + r_2 N_2 + r_4 N_4 + r_6 N_6 + r_5 N_5 \quad (3a)$$

in which the r's ($\geqq 1$), which can be called *reserve* factors, explicitly allow for the possibility that a "real" cotransport system may have more carrier states than the six depicted in Figs. 1 and 2 (*see* Appendix II). For immediate purposes, it is sufficient to ignore this possibility and assume that all r's are unity. Then,

$$N \equiv N_3 + N_1 + N_2 + N_4 + N_6 + N_5. \quad (3b)$$

Table 1. Expansion of terms in Eqs. (4), (5), and (6)[a]

FIRST ON (Fig. 1A,B)

$$|\mathbf{M}_6| = k_{13}k_{35}k_{56}[k_{46}(k_{21}+k_{24}) + k_{42}k_{21}] + k_{46}k_{24}k_{12}[k_{31}(k_{53}+k_{56}) + k_{35}k_{56})$$

$$A_6 = k_{46}(k_{24}+k_{21})[k_{65}k_{53}(k_{13}+k_{31}) + k_{13}k_{35}(k_{65}+k_{56})] + (k_{42}k_{21}k_{13}+k_{46}k_{24}k_{12})\cdot [k_{65}(k_{35}+k_{53}) + k_{35}k_{56}] + k_{53}k_{65}k_{12}k_{31}(k_{46}+k_{42}+k_{24}) + k_{46}k_{24}k_{12}k_{31}\cdot (k_{53}+k_{56}+k_{65}) + k_{65}k_{42}k_{21}k_{31}k_{53}$$

$$k^oB_6 = k^o_{64}\{(k_{56}+k_{53})[k_{42}k_{21}(k_{13}+k_{31}) + k_{12}k_{31}(k_{42}+k_{24})] + k_{35}k_{56}[(k_{42}+k_{24})(k_{12}+k_{13}) + k_{42}k_{21}] + k_{21}k_{13}k_{35}(k_{42}+k_{56})\}$$

First off (Fig. 1B)	Last off (Fig. 1A)
$P = k_{42}k_{21}k_{13}$	$k_{42}k_{21}k_{13}k_{35}$
$\|^*\mathbf{M}\| = k_{46}k_{24}(k_{12}+k_{13}) + k_{21}k_{13}(k_{46}+k_{42})$ (i)	(i) $k_{35}[k_{46}k_{24}(k_{12}+k_{13}) + k_{21}k_{13}(k_{46}+k_{42})] + k_{46}k_{24}k_{12}k_{31}$
	(ii) $k_{46}[k_{13}k_{35}(k_{24}+k_{21}) + k_{24}k_{12}(k_{31}+k_{35})] + k_{42}k_{21}k_{13}k_{35}$

LAST ON (Fig. 1C,D)

$$|\mathbf{M}_4| = k_{35}k_{56}k_{64}[k_{24}(k_{12}+k_{13}) + k_{21}k_{13}] + k_{24}k_{12}k_{31}[k_{53}(k_{65}+k_{64}) + k_{56}k_{64})$$

$$A_4 = k_{24}(k_{12}+k_{13})[k_{46}k_{65}(k_{35}+k_{53}) + k_{35}k_{56}(k_{46}+k_{64})] + (k_{21}k_{13}k_{35}+k_{24}k_{12}k_{31})\cdot [k_{46}(k_{56}+k_{65}) + k_{56}k_{64}] + k_{65}k_{46}k_{31}k_{53}(k_{24}+k_{21}+k_{12}) + k_{24}k_{12}k_{31}k_{53}\cdot (k_{65}+k_{64}+k_{46}) + k_{46}k_{21}k_{13}k_{53}k_{65}$$

$$k^oB_4 = k^o_{42}\{(k_{65}+k_{64})[k_{21}k_{13}(k_{35}+k_{53}) + k_{31}k_{53}(k_{21}+k_{12})] + k_{56}k_{64}[(k_{21}+k_{12})(k_{31}+k_{35}) + k_{21}k_{13}] + k_{13}k_{35}k_{56}(k_{21}+k_{64})\}$$

First off (Fig. 1D)	Last off (Fig. 1C)
$P = k_{21}k_{13}$	$k_{21}k_{13}k_{35}$
$\|^*\mathbf{M}\| = k_{24}(k_{12}+k_{13}) + k_{21}k_{13}$ (i) $k_{13}(k_{24}+k_{21}) + k_{24}k_{12}$ (ii)	(ii) $k_{13}k_{35}(k_{24}+k_{21}) + k_{24}k_{12}(k_{31}+k_{35})$

[a] Subscripting nomenclature used in this table is taken directly from the legend to Fig. 2. The algebraic expansions have been written in a fashion to emphasize similarities between corresponding terms obtained for different conditions. For example, $|\mathbf{M}_4|$, A_4, and k^oB_4 in the lower half table can be derived from $|\mathbf{M}_6|$, A_6, and k^oB_6 (upper half table) by rotational symmetry. Also, two equivalent forms of $|^*\mathbf{M}|$ (designated *i*, *ii*) are given for the first on-last off case and for the last on-first off case, in order to emphasize their direct relation to the other three cases. The relationships among the four forms of P can be seen by simple inspection.

(The order here: 3, 1, etc., is chosen simply to coincide with the sequence in the cycle diagrammed in Fig. 2 and to facilitate comparison with the matrix notation in Appendix I).

Formal Development of the Model

The most important relationship that emerges from algebraic formulation of the model in Fig. 2*A* is that influx of isotopically labeled substrate (*S) obeys a hyperbolic relationship, as a function of the external substrate concentration ($[S]_o$). Specifically, when experiments are carried out with the internal specific activity ($[^*S]_i/[S]_i$) equal to zero (as usual for initial-rate measurements), it can be shown that unidirectional substrate influx is given by

$$J_S = \frac{J_{max}[S]_o}{K_m + [S]_o} \tag{4}$$

in which $[S]_o$ and its influx (counterclockwise flow) are marked by the isotope, *S. Maximal velocity has the form

$$J_{max} = N \frac{P|\mathbf{M}_j|}{B_j|^*\mathbf{M}|} \tag{5}$$

and the Michaelis constant has the form

$$K_m = \frac{A_j}{k^o B_j}. \tag{6}$$

The derivation of these relationships is provided in Appendix I, but the meaning of the several terms in Eqs. (5) and (6) can be briefly stated as follows:

N = Total carrier (usually specified as a surface concentration, such as moles/sq. meter), given by Eq. (3) above.

P = Product of all forward reaction constants from the first *S-bound state through *S release.

$A_j + k^o B_j[S]_o = |\mathbf{M}|$ = characteristic determinant for the whole carrier system. $|\mathbf{M}|$ is the same for all binding sequences, but the composition of A_j (21 terms) and B_j (15 terms) differs, depending on whether k^o_{64} or k^o_{42} is extracted. $j = 4$ or 6.

$|\mathbf{M}_j|$ = Determinant associated with the S-binding form of the carrier.

$|^*\mathbf{M}|$ = Characteristic determinant for the isotopically labeled portion of the carrier system.

The explicit algebraic expansions of these terms are listed in Table 1. Thus, Eqs. (4), (5), and (6) – taken together with Table 1, Eq. (1) or (2), and the parameter-substrate correspondence listed in the legend to Fig. 2 – give the principal relationships needed for calculating effects of both membrane potential and driver-ion concentration on the kinetics of substrate transport by a simple Class-I cotransport system. The relationships cover all cases of 1:1 (ion/neutral substrate) stoichiometry, for either charge sign of the carrier, and for all four ordered binding sequences. However, the models can easily be modified to include cases where $|z| > 1$.

Simplification of the Model with Experimentally Attainable Conditions

Clearly the complete rate relationship, Eq. (4) expanded by Eqs. (5) and (6) and Table 1, is too complex to be very informative – on inspection – about the effect of varying any one parameter. Therefore, in order to explore the dependence of the K_m or J_{max} (for substrate transport) upon another parameter, such as the extracellular concentration of driver ions, it is useful to obtain preliminary information about the likely overall effect of changing that parameter. Extracting such information can be greatly facilitated by imposing physiologically verifiable conditions on the model, *for test purposes only*, and prior to numerical analysis of the full rate-equation. Three different conditions, which have proven particularly useful in this regard, are set out below, along with the simplified equations for J_{max} and K_m which result from their use. Only the "FL" model (first on-last off; Fig. 1*A*), with the doubly loaded form of the carrier assumed to be charged ($FL+$), is treated explicitly below; the corresponding equations for the "$FF+$", "$LL+$", and "$LF+$" models, and for the unloaded carrier charged ($FL-$, $FF-$, etc.) are given in Appendix I, Table A1.

1) "Saturating $\Delta\psi$": That the membrane potential is large enough (cell interior negative) to be saturating in its effect on flux. The simplifying condition that $k_{12} \gg k_{21}$ can then be introduced into the complete rate equation. Previous calculations (Hansen et al., 1981) have shown that a displacement of about 100 mV negative to the carrier equilibrium potential is sufficient for saturation with respect to $\Delta\psi$. Since many cells using H^+– coupled substrate transport have resting membrane potentials in the neighborhood of (–) 200 mV, this restriction can be achieved without excessive manipulation of substrate and driver-ion gradients. This notion is supported by experimental evidence on two H^+ cotransport systems, indicating that $\Delta\psi$ is saturating at all normal resting potentials (Hansen & Slayman, 1978; Felle, 1981). The resulting expansion of Eq. (5), with $k_{12} \gg k_{21}$, is

$$\frac{J_{max}}{N} = \frac{[H^+]_o k^o_{42} k_{13} k_{35} k_{56}}{[H^+]_o k^o_{42}[(k_{13}+k_{31})(k_{53}+k_{56})+k_{35}(k_{13}+k_{56})]+k_{13}k_{35}k_{56}} \tag{7a}$$

$$= \frac{k_{42} k_{13} k_{35} k_{56}}{[H^+]_i k^o_{31} k_{42}(k_{53}+k_{56})+k_{42}k_{13}(k_{35}+k_{53}+k_{56})+k_{35}k_{56}(k_{42}+k_{13})} \tag{7b}$$

in which the two different forms are written to emphasize their dependence on either external driver ion $[H^+]_o$ (7a) or internal driver ion $[H^+]_i$ (7b), according to the identities in the legend to Fig. 2. The corresponding expansion of Eq. (6) is

$$K_m = \frac{\{[H^+]_o k^o_{42} + k_{46}\}\{k_{53}k_{65}(k_{13}+k_{31})+k_{13}k_{35}(k_{56}+k_{65})\}}{k^o_{64}\{[H^+]_o k^o_{42}[(k_{13}+k_{31})(k_{53}+k_{56})+k_{35}(k_{13}+k_{56})]+k_{13}k_{35}k_{56}\}} \tag{8a}$$

$$= \frac{[H^+]_i k^o_{31} k_{53} k_{65}(k_{46}+k_{42})+k_{13}(k_{46}+k_{42})[k_{35}(k_{56}+k_{65})+k_{65}k_{53}]}{k^o_{64}\{[H^+]_i k^o_{31} k_{42}(k_{53}+k_{56})+k_{42}k_{13}(k_{35}+k_{53}+k_{56})+k_{35}k_{56}(k_{42}+k_{13})\}}. \tag{8b}$$

Again, the two forms are written to emphasize their dependence on the external or internal driver-ion concentration, with Eq. (8a) and (8b) corresponding to the J_{max} expressions of (7a) and (7b), respectively. As is to be expected from the assumption of saturating membrane potential, the reaction constants k_{12} and k_{21}, for the voltage-sensitive steps, do not appear in Eqs. (7) and (8). From Eq. (1), it can be seen that k_{21} becomes very large so that it cancels out of the numerators and denominators of all expressions, while k_{12} approaches zero and drops out. Equations (7a, b) are rearrangements of Appendix Eq. (A13a), and Eqs. (8a, b) are rearrangements of Appendix Eq. (A13b).

2) "Zero Trans-Ligand": That the intracellular concentration of coupled substrate is zero. This assumption resembles that made for calculating isotope fluxes, but is stronger in setting both $[S]_i$ and $[H^+]_i$ at zero. (For proton-coupled transport systems, this is not a strictly attainable condition, though it can be approximated if internal pH is high enough not to be rate limiting. For sodium-coupled systems, the condition can also be attained in practice if $[Na^+]_i \ll$ the inhibition constant for Na^+, K_I.) This allows both the reaction constants k_{53} and k_{31} to be set at zero, so that Eq. (5) can then be written

$$\frac{J_{max}}{N} = \frac{[H^+]_o k^o_{42} k_{21} k_{13} k_{35} k_{56}}{[H^+]_o k^o_{42}[k_{35}k_{56}(k_{21}+k_{12}+k_{13})+k_{21}k_{13}(k_{35}+k_{56})]+k_{35}k_{56}[k_{24}(k_{12}+k_{13})+k_{21}k_{13}]} \tag{9a}$$

$$= \frac{k^o_{21}\exp(-u/2)\,k_{42}k_{13}k_{35}k_{56}}{k^o_{21}\exp(-u/2)[k_{42}k_{56}(k_{13}+k_{35})+k_{13}k_{35}(k_{42}+k_{56})]+(k^o_{12}\exp(u/2)+k_{13})\,k_{35}k_{56}(k_{42}+k_{24})}. \tag{9b}$$

In this case the expansion of J_{max} has been written in two ways, emphasizing its dependence either on the external driver-ion concentration (9a) or on the membrane potential (9b). The corresponding formulas for K_m are:

$$K_m = \frac{[H^+]_o k^o_{42} k_{21} k_{13} k_{35}(k_{56}+k_{65})+k_{46}k_{35}(k_{56}+k_{65})[k_{24}(k_{12}+k_{13})+k_{21}k_{13}]}{k^o_{64}\{[H^+]_o k^o_{42}[k_{35}k_{56}(k_{21}+k_{12}+k_{13})+k_{21}k_{13}(k_{35}+k_{56})]+k_{35}k_{56}[k_{24}(k_{12}+k_{13})+k_{21}k_{13}]\}}. \tag{10a}$$

$$= \frac{[k^o_{21}\exp(-u/2)\,k_{13}(k_{46}+k_{42})+k^o_{12}\exp(u/2)\,k_{46}k_{24}+k_{46}k_{24}k_{13}]\cdot[k_{35}(k_{56}+k_{65})]}{k^o_{64}\{k^o_{21}\exp(-u/2)[k_{42}k_{56}(k_{13}+k_{35})+k_{13}k_{35}(k_{42}+k_{56})]+(k^o_{12}\exp(u/2)+k_{13})\,k_{35}k_{56}(k_{42}+k_{24})\}}. \tag{10b}$$

Equations (9a, b) and (10a, b) are rearrangements of Appendix Eqs. (A14a) and (A14b), respectively.

3) "Saturating Cis-Driver Ion": That the extracellular concentration of the driver ion is high enough to make the reaction (Fig. 1*A*) $SX + H^+_o \rightleftharpoons SXH^+$ at the outer surface of the membrane limited only by the availability of the carrier SX. The reaction constant k_{42} is then very large, and

$$\frac{J_{max}}{N} = \frac{k^o_{21}\exp(-u/2)\,k_{13}k_{35}k_{56}}{k^o_{21}\exp(-u/2)[k_{31}(k_{53}+k_{56})+k_{35}k_{56}+k_{13}(k_{35}+k_{53}+k_{56})]+k^o_{12}\exp(u/2)[k_{31}(k_{53}+k_{56})+k_{35}k_{56}]+k_{13}k_{35}k_{56}}$$

$$= \frac{k_{21}k_{13}k_{35}k_{56}}{[H^+]_i k^o_{31}(k_{53}+k_{56})(k_{21}+k_{12})+k_{21}k_{13}(k_{35}+k_{53}+k_{56})+k_{35}k_{56}(k_{21}+k_{12}+k_{13})}. \tag{11a, 11b}$$

In this case the two expressions for J_{max} are written to show their dependence on membrane potential and the intracellular concentration of driver ion, respectively. Finally, K_m can be written for this case as

$$K_m = \frac{k^o_{21}\exp(-u/2)[k_{13}k_{35}(k_{56}+k_{65})+k_{53}k_{65}(k_{13}+k_{31})]+k^o_{12}\exp(u/2)\,k_{31}k_{53}k_{65}}{k^o_{64}\{k^o_{21}\exp(-u/2)[k_{31}(k_{53}+k_{56})+k_{35}k_{56}+k_{13}(k_{35}+k_{53}+k_{56})]+k^o_{12}\exp(u/2)[k_{31}(k_{53}+k_{56})+k_{35}k_{56}]+k_{13}k_{35}k_{56}\}} \tag{12a}$$

$$= \frac{[H^+]_i k^o_{31}k_{53}k_{65}(k_{21}+k_{12})+k_{21}k_{13}[k_{65}(k_{35}+k_{53})+k_{35}k_{56}]}{[H^+]_i k^o_{31}(k_{53}+k_{56})(k_{21}+k_{12})+k_{21}k_{13}(k_{35}+k_{53}+k_{56})+k_{35}k_{56}(k_{21}+k_{12}+k_{13})}. \tag{12b}$$

Equations (11a, b) and (12a, b) are rearrangements of Appendix Eqs. (A15a) and (A15b), respectively.

In the description that follows, our operating procedure has been to inspect the above equations in order to draw tentative rules describing the effects - on J_S, J_{max}, or K_m - of separately varying the extracellular driver-ion concentration, the membrane potential, or the intracellular driver-ion concentration. We have then tested the rules for their range of general validity, using the full forms of Eqs. (4)-(6) (plus Table 1) for numerical computations. In all cases, the anticipated responses were obtained, thereby demonstrating that the rules that emerge from the simplified cases are general and not restricted to special physiological conditions.

Results

In the kinetic models of Fig. 1, determination of how an experimental change of driver-ion concentration (or membrane potential) will affect the kinetics of substrate influx rests on the relative magnitudes of the reaction constants set out in Fig. 2. With a few exceptions, it is possible to generate essentially pure changes in J_{max}, pure changes in K_m, or mixed changes in J_{max} and K_m by proper ordering of the reaction constants. This holds true whether the independent variable is extracellular driver-ion concentration, intracellular driver-ion concentration,

Table 2. Summary list of conditions which cause selected changes of J_{max} and K_m for substrate influx, when driver-ion concentrations ($[H^+]_o$ or $[H^+]_i$) or membrane potential ($\Delta\psi$) are varied[a]

Experimental conditions	Variable	Site of charge transfer	Column #	1	2	3	4	Equation #'s	Row #
			Models	J_{max} alone	K_m alone	J_{max} and K_m parallel	J_{max} and K_m opposite		
1) $\Delta\psi$ negative saturating	i) $[H^+]_o$	a) Loaded carrier (+)	FL, FF	$k_{13}k_{35}k_{56}$, $k_{46} > k^o_{42}[H^+]_o$	$k_{46} > k^o_{42}[H^+]_o > k_{13}k_{35}k_{56}$	$k_{13}k_{35}k_{56} > k^o_{42}[H^+]_o > k_{46}$	$k_{46} > k^o_{42}[H^+]_o \simeq k_{13}k_{35}k_{56}$	A13, 7a, 8a	1
			LL, LF	$k_{65} > k^o_{64}[H^+]_o$	$k_{46} > k^o_{64}[H^+]_o > k_{65}$, k_{35}	$k_{65} > k^o_{64}[H^+]_o > k_{46}$	$k_{46} > k^o_{64}[H^+]_o \simeq k_{65}$	A16	2
		b) Unloaded carrier (-)	FL, FF	k_{24}, $k_{46} > k^o_{42}[H^+]_o$	$k_{46} > k^o_{42}[H^+]_o > k_{21}$, k_{24}	$k_{24} > k^o_{42}[H^+]_o > k_{46}$	$k_{46} > k^o_{42}[H^+]_o \simeq k_{24}$	A20, A21	3
			LL, LF	$k_{21}k_{13}k_{35}$, $k_{46} > k^o_{64}[H^+]_o$	$k_{46} > k^o_{64}[H^+]_o > k_{21}k_{13}k_{35}$	$k_{21}k_{13}k_{35} > k^o_{64}[H^+]_o > k_{46}$	$k_{46} > k^o_{64}[H^+]_o \simeq k_{21}k_{13}k_{35}$	A24, A25	4
	ii) $[H^+]_i$	a) Loaded carrier (+)	FL, LL	$k^o_{31}[H^+]_i > k_{13}$, k_{35}	$k_{35} > k^o_{31}[H^+]_i >> k_{13}$	$k_{65} > k^o_{31}[H^+]_i > k_{13}$, k_{35}	$k_{35} \simeq k^o_{31}[H^+]_i > k_{13}$	A13, 7b, 8b	5
			FF, LF	$k^o_{53}[H^+]_i > k_{35}$, k_{56}	$k_{56} > k^o_{53}[H^+]_i >> k_{13}$ or k_{35}	$k^o_{53}[H^+]_i > k_{35}$, $k_{56} >> k_{65}$	$k_{56} \simeq k^o_{53}[H^+]_i > k_{13}$ or k_{35}	A16	6
		b) Unloaded carrier (-)	FL, LL	$k^o_{31}[H^+]_i > k_{13}$, k_{35}	$k_{13} > k^o_{31}[H^+]_i >> k_{35}$	$k_{21} > k^o_{31}[H^+]_i > k_{13}$, k_{35}	$k_{13} \simeq k^o_{31}[H^+]_i > k_{35}$	A20, A21	7
			FF, LF	Not sensitive	Not sensitive	Not sensitive	Not sensitive	A24, A25	8
2) Zero trans-ligand	i) $[H^+]_o$		FL, FF	k_{24}, $k_{46} > k^o_{42}[H^+]_o$	$k_{46} > k^o_{42}[H^+]_o > k_{24}$, k_{13}	$k_{24} > k^o_{42}[H^+]_o >> k_{46}$	$k_{46} > k^o_{42}[H^+]_o \simeq k_{24}$	A14, 9a, 10a	9
			LL, LF	k_{46}, $k_{65} > k^o_{64}[H^+]_o$	$k_{46} > k^o_{64}[H^+]_o > k_{13}$	$k_{65} > k^o_{64}[H^+]_o > k_{46}$	$k_{46} > k^o_{64}[H^+]_o \simeq k_{65}$	A17	10
	ii) $\Delta\psi$	a) Loaded carrier (+)	FL, FF	$k^o_{12}e^{U/2} > k_{24} >> k^o_{21}e^{-U/2}$	$k_{24} > k^o_{21}e^{-U/2} >> k_{56}$	$k_{42}k_{13}k_{35}k_{56} > k^o_{21}e^{-U/2} > k_{24}$	$k_{24} > k^o_{21}e^{-U/2} \geq k_{56}$	A14, 9b, 10b	11
			LL, LF	k_{24}, $k_{13} > k^o_{21}e^{-U/2}$, $k^o_{12}e^{U/2}$	$k_{24} > k^o_{21}e^{-U/2} > k_{56}$	$k_{13}k_{35}k_{56}k_{64} > k^o_{21}e^{-U/2} > k_{24}$	$k_{24} >$ all others	A17	12
		b) Unloaded carrier (-)	FL, FF	$k_{42}k_{21}k_{13}k_{35} > k^o_{56}e^{U/2} \simeq k^o_{65}e^{-U/2}$	$k^o_{65}e^{-U/2} > k^o_{56}e^{U/2} > k_{42}k_{21}k_{13}k_{35}$	$k_{42}k_{21}k_{13}k_{35} > k^o_{56}e^{U/2} > k^o_{65}e^{-U/2}$	$k^o_{65}e^{-U/2} > k^o_{56}e^{U/2} \simeq k_{42}k_{21}k_{13}k_{35}$	A22	13
			LL, LF	$k^o_{65}e^{-U/2} > k^o_{56}e^{U/2} \simeq k_{21}k_{13}k_{35}$	$k^o_{65}e^{-U/2} > k^o_{56}e^{U/2} >> k_{21}k_{13}k_{35}$	$k_{21}k_{13}k_{35} > k^o_{56}e^{U/2} > k^o_{65}e^{-U/2}$	$k_{64} > k^o_{65}e^{-U/2} >> k^o_{56}e^{U/2}$	A26	14
3) $[H^+]_o$ Saturating	i) $[H^+]_i$		FL	$k^o_{31}[H^+]_i > k_{13}$, k_{35}	$k_{35} > k^o_{31}[H^+]_i >> k_{13}$	$k_{56} >> k_{65}$, $k^o_{31}[H^+]_i > k_{13}$, k_{35}	$k_{35} \simeq k^o_{31}[H^+]_i > k_{13}$	A15, 11b, 12b	15
			FF	$k^o_{53}[H^+]_i > k_{13}$, k_{35}	$k_{56} > k^o_{53}[H^+]_i >> k_{13}$	$k_{56} >> k_{65}$, $k^o_{53}[H^+]_i > k_{13}$, k_{35}	$k_{56} \simeq k^o_{53}[H^+]_i > k_{13}$	A15	16
			LL	$k^o_{31}[H^+]_i > k_{13} >> k_{35}$	$k_{13} > k^o_{31}[H^+]_i >> k_{35}$	$k^o_{31}[H^+]_i > k_{13}$, $k_{35} >> k_{12}$	$k_{13} \simeq k^o_{31}[H^+]_i >> k_{35}$	A18	17
			LF	Not sensitive	Not sensitive	Not sensitive	Not sensitive	A19	18
	ii) $\Delta\psi$	a) Loaded carrier (+)	FL, FF	$k^o_{12}e^{U/2} > k_{13} >> k^o_{21}e^{-U/2}$	$k_{13} >> k^o_{12}e^{U/2} > k^o_{21}e^{-U/2} > k_{35}$	$k_{13} > k^o_{21}e^{-U/2} >> k_{65}$, $k^o_{12}e^{U/2}$	$k_{13} \simeq k^o_{12}e^{U/2} >> k^o_{21}e^{-U/2}$	A15, 11a, 12a	19
			LL, LF	$k_{13} > k^o_{21}e^{-U/2}$, $k^o_{12}e^{U/2}$	$k_{31}, k_{24} >> k^o_{21}e^{-U/2} > k_{13} >> k^o_{12}e^{U/2}$	$k^o_{12}e^{U/2} > k^o_{21}e^{-U/2}, k_{13} >> k_{24}$	$k_{24} > k^o_{21}e^{-U/2} \simeq k_{13} > k^o_{12}e^{U/2}$	A18, A19	20
		b) Unloaded carrier (-)	FL, FF	$k_{21}k_{13}k_{35} > k^o_{56}e^{U/2} \simeq k^o_{65}e^{-U/2}$	$k^o_{65}e^{-U/2} >> k^o_{56}e^{U/2} > k_{13}, k_{53}$	$k_{53} > k^o_{56}e^{U/2} >> k^o_{65}e^{-U/2}$	k_{53}, $k^o_{65}e^{-U/2} > k^o_{56}e^{U/2}$	A23	21
			LL, LF	Not sensitive	Not sensitive	Not sensitive	Not sensitive	A27, A28	22

[a] The conditions listed are not necessarily unique in generating the selective effects reported for a single model, as reference to the appropriate equations will show. For the sake of compactness, we define a new voltage parameter (U), in this table, equal to "zu" in the main text.

or membrane potential; it holds for either of the four binding orders; and it holds whether charge transfer occurs with the unloaded (−) or with the doubly loaded (+) carrier. Some examples of the required ordering of reaction constants are listed in Table 2. The graphic development which follows is based on the "FL+" model alone (Fig. 1*A*). Preliminary guesses were made from the limiting conditions of Eqs. (7)–(12), and numerical computations were carried out using Eqs. (4)–(6), supplemented from Table 1 (for the "FL+" case).

It is important to note that absolute values of reaction constants are immaterial for the present kind of modelling; what matters is only their size relative to each other. Therefore, for simplicity in the numerical computations, as many constants as possible were fixed at unity (*see* Part *A* of Figs. 3, 5, etc.). In the case of ligand-binding reactions, each assigned value should be understood as an initial value, in which the concentration component was started at 1 (e.g., $[H^+]_o=1$, in $k_{42}=[H^+]_o k^o_{42}$); for computation, the product was then changed in direct proportion to the desired values of ligand concentration.

In assigning values to the reaction constants in the numerical examples, we have not imposed restrictions concerning the sites of exergonic and endergonic reactions. This is consistent with the view (Hill & Eisenberg, 1981) that energetic transitions of the carrier need not be associated with the reactions coupled to solute movement *per se*, but can be localized in alternate parts of the carrier reaction cycle. For the sake of consistency between models, each of the models discussed in the next section is initially poised at equilibrium, before we consider specific changes in driving force involving each of the components $[H^+]_o$, $\Delta\psi$, and $[H^+]_i$. The equilibrium condition is simply that the products of the clockwise and counter-clockwise reaction constants are equal.

I. Variation of Extracellular Driver Ion Concentration

A. Selective Effects of $[H^+]_o$ *on* K_m

1. *Membrane Potential Negative and Saturating.* Inspection of Eq. (7a) shows that J_{max} will be insensitive to changes of $[H^+]_o$ when the voltage-insensitive reactions in forward transport (counterclockwise, in Fig. 2) are slow: that is, when the product $k_{13}k_{35}k_{56}$ is small, so

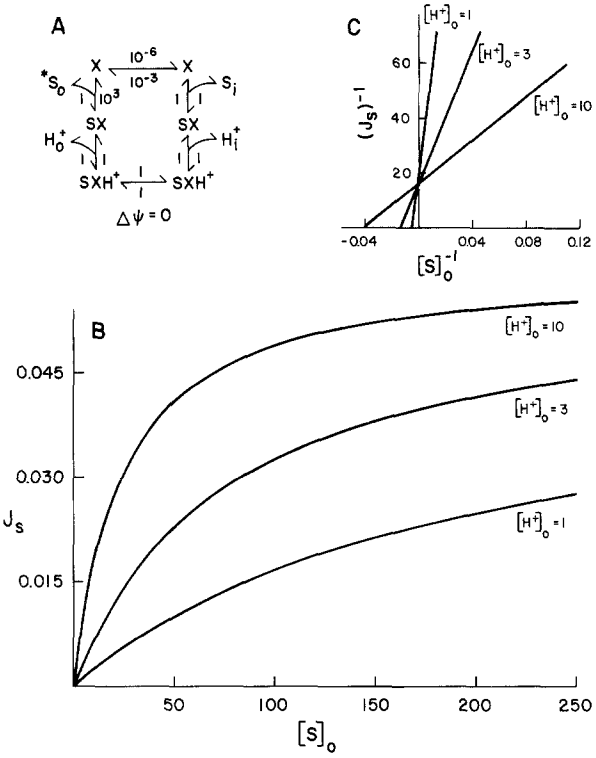

Fig. 3. Selective effect of external driver-ion concentration on K_m. (*A*): Carrier model "FL+", poised at equilibrium, and capable of exhibiting a selective effect of driver ion on the K_m for transport of isotopic S from outside (left) to inside (right). Values for the individual reaction constants are shown in the model. Most are set to unity, and others were assigned according to the criteria outlined in the text and Table 2. (*B*): Velocity-concentration plots for transport of isotopic S, at three different driver ion concentrations. Membrane potential was set to zero, and *N* set to 1. $[S]_o$ was adjusted through changes in k_{64} and $[H^+]_o$ through changes in k_{42} (as shown in Fig. 2). (*C*): Double reciprocal plots of the curves in *B*

that the concentration terms cancel from numerator and denominator. If at the same time substrate dissociation at the membrane exterior is rapid (k_{46} large), then the numerator of K_m in Eq. (8a) will be insensitive to $[H^+]_o$, but the denominator of K_m will be proportional to $[H^+]_o$. In other words, K_m will *decrease* in proportion to *increasing* external driver-ion concentration.

2. *Zero Trans-Ligand.* This case is very similar to that just discussed. From Eq. (9a), J_{max} will be insensitive to $[H^+]_o$ when both doubly loaded forms of the carrier are slow to dissociate: i.e., when k_{24} and k_{13} are small. Again, if substrate dissociation at the membrane exterior is rapid (k_{46} large), K_m will vary in inverse proportion to $[H^+]_o$ (Eq. (10a)].

3. *Computations.* Conditions obtained in 1 and 2 were used as a guideline to construct Fig. 3. As shown in part *A*, all reaction constants, except k_{65}, k_{56}, and k_{46}, were set at unity. The product $k_{13}k_{35}k_{56}$ was kept small by assigning k_{56} the value 10^{-3}; and k_{46} was set high, at 10^3. Membrane potential was put at zero, which is *not* a simplifying condition – but rather a more general condition than that discussed in 1 – since it retains both k^o_{12} and k^o_{21} in Eqs. (5) and (6). Finally, to poise the system at equilibrium, k_{65} was assigned the value 10^{-6} for the initial conditions ($[S]_o = [H^+]_o = 1$).

Figure 3*B* shows the resultant computations of transport velocity, versus substrate concentration, at three different concentrations of driver ion. From the double reciprocal plot of the same results (Fig. 3*C*), it is clear that the primary effect of raising $[H^+]_o$ is indeed to reduce the K_m for substrate transport. The calculations were carried over nearly three log units of concentration for $[H^+]_o$, and summary results are plotted in Fig. 4. Linear proportionality between declining K_m and rising $[H^+]_o$ holds for at least two log units of concentration (and K_m). Over the same concentration range, J_{max} remains nearly insensitive to $[H^+]_o$, varying less than 25% from the value (5×10^{-2}) for equilibrium conditions. [As $[H^+]_o$ is raised above 1000, for the conditions in Fig. 4, J_{max} begins to decline. The reason for this cannot be seen from the simplified Eqs. (7a) and (9a), but substitution of the reaction constants in Fig. 3*A* into the full rate-equation reveals only a single significant term for $[H^+]_o k^o_{42}$ in the numerator, whereas the denominator varies as the square of $[H^+]_o k^o_{42}$ at these very high concentrations. This generates an interesting case, not dealt with elsewhere in this paper, where a rise in the concentration of driver ion results in a *simultaneous decline* of both J_{max} and K_m.]

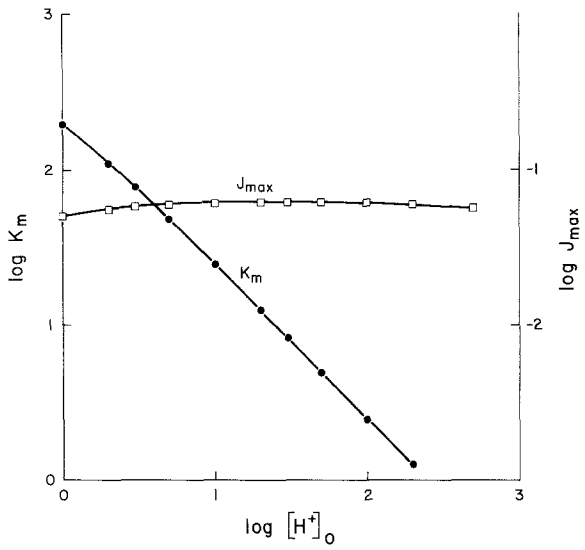

Fig. 4. Selective effects of external driver-ion concentration ($[H^+]_o$) on K_m can hold over at least two orders of magnitude of $[H^+]_o$. Individual points are calculated from model in Fig. 3*A*, and curves are drawn by eye. Point at which electrochemical gradient of driver ion is zero is at far left of figure ($[H^+]_o = [H^+]_o = 1$, $\Delta\psi = 0$). Note negligible effects of $[H^+]_o$ on J_{max}. As predicted by Eq. (7a), in conjunction with the condition in Table 2 (Row 1, Column 2), K_m shows simple inverse proportionality with $[H^+]_o$: the slope of the log-log plot is negative and close to unity

B. Selective Effects of $[H^+]_o$ *on* J_{max}

With membrane potential assumed to be negative and saturating, Eq. (7a) shows that J_{max} will vary in direct proportion to $[H^+]_o$, when the product of voltage-insensitive reaction constants, $k_{13}k_{35}k_{56}$, is large enough that the $[H^+]_o$ terms of the denominator can be neglected. This condition is opposite to that required for a selective effect on K_m, but accords with intuition in making H^+ binding rate-limiting to the forward operation of the transport cycle. If k_{46} is also large, then [Eq. (8a)] K_m will be insensitive to $[H^+]_o$. Analogous circumstances obtain when the condition of zero trans-ligand is assumed; then Eqs. (9a) and (10a) demonstrate that k_{24} and k_{46} must be large.

Numerical results, calculated from Eqs. (4)–(6) and displayed in Fig. 5, buttress these conclusions. As shown in Fig. 5*A*, k_{42} was set at 10^{-3} for $[H^+]_o = 1$, in order to make H^+ binding rate limiting. For symmetry, the same value was used for H^+ binding at the cytoplasmic surface of the membrane. The product $k_{13}k_{35}k_{56}$ was made large by letting k_{56} equal 10^3. And finally, overall equilibrium was imposed, for $[S]_o = [H^+]_o = 1$, by fixing k_{65} also at 10^3. Figure 5*B* and *C* shows the Cartesian and double-reciprocal plots of substrate-flux versus concentration; the pure effect on J_{max} is evident. Figure 6 shows plots of K_m and J_{max} extended over two log units of concentration for driver ion.

C. Parallel changes of K_m *and* J_{max}

Equations (7a) and (8a), for saturating negative membrane potential, yield parallel changes of K_m and J_{max} when both denominators are dominated by the $[H^+]_o$-independent term

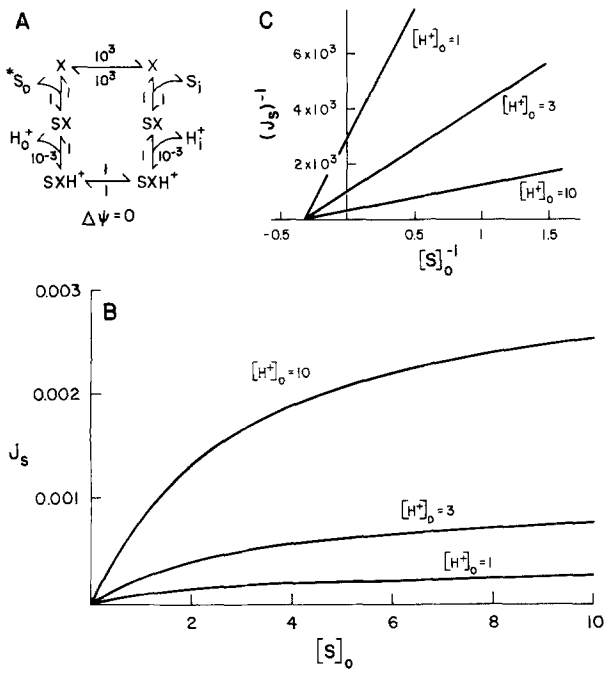

Fig. 5. Selective effect of $[H^+]_o$ on J_{max}. (*A*): "FL+" model, at equilibrium, with values of the reaction constants as shown. Those not set to unity were assigned according to the criteria outlined in the text and Table 2. For the purposes of the modelling, all ligand concentrations are set to unity at equilibrium, so that those marked "10^{-3}" represent k^o_{42} and k^o_{31}, with $[H^+]$ excluded (*see* Fig. 2). (*B*): Velocity concentration plots for transport of isotopic S at three different $[H^+]_o$. Manipulations of model and other conditions as for Fig. 3. (*C*): Double reciprocal plots of curves in *B*

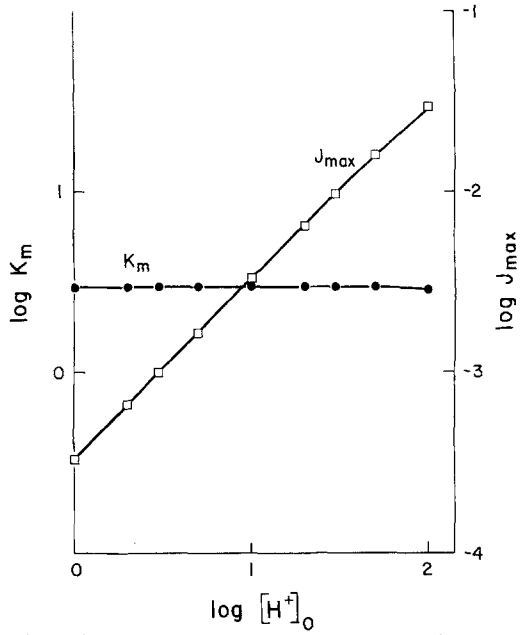

Fig. 6. Log-log plots demonstrating simple proportionality between J_{max} and $[H^+]_o$ over two orders of magnitude of $[H^+]_o$. K_m shows no dependence on $[H^+]_o$ over this range. Results of calculations, based on model in Fig. 5*A*, are shown as points; curves are drawn by eye through the points

$k_{13}k_{35}k_{56}$ and, at the same time, k_{46} is negligible in the numerator of Eq. (8a). Thus, $k_{13}k_{35}k_{56}$ must be large, while k_{46} must be small. Equations (9a) and (10a), for zero transligand, will yield the same result when k_{24} is very large and k_{46} is very small, relative to $[H^+]_o k^o_{42}$.

Appropriate numerical results are displayed in Fig. 7, where again the double reciprocal plot (Fig. 7C) emphasizes the concomitant rise of K_m and J_{max}. The product $k_{13}k_{35}k_{56}$ was made large by setting k_{56} equal to 10^4; and k_{46} was assigned the small value 10^{-3}. In order for the term $k_{13}k_{35}k_{56}$ to dominate the denominator, $[H^+]_o k^o_{42}$ must be much smaller than this product, since each of the reaction constants is also a multiplier of $[H^+]_o k^o_{42}$. Thus $[H^+]_o k^o_{42}$ was raised from a starting value of 10^{-3}, and the other reaction constants in Fig. 7*A* ($k_{31} = 10^{-3}$; $k_{53} = 10^3$; $k_{65} = 10^4$) have been chosen both to generate identical ligand dissociation constants on both sides of the membrane and to poise the system at equilibrium. Log-log plots of J_{max} and K_m versus $[H^+]_o$ are given in Fig. 8, for a 500-fold concentration range. Both parameters rise monotonically over this range, but with different (and varying) slopes, as is also implied by the changing slopes in the double reciprocal plots (Fig. 7C). The parallel between K_m and J_{max} improves at high $[H^+]_o$, with the increasing disparity between $[H^+]_o k^o_{42}$ and k_{46}.

This particular result emphasizes the flexibility of the present models in comparison with those which incorporate equilibrium binding. For the "FL" sequence, equilibrium binding models appear incapable of describing a rise in K_m with driver-ion concentration (*cf.* Turner, 1981), since there is no term incorporating driver-ion concentration into the numerator of K_m. As can be seen in Table 1, A_6, which constitutes the numerator of K_m, does contain $[H^+]_o k^o_{42}$ terms, but *these drop out* when k_{65}, k_{56}, k_{12} and k_{21} are all made small. In contrast, the many recorded instances of parallel rises in J_{max} *and* K_m with external driver-ion concentration (Cohen, 1980) are readily explained by FL models not subject to the rapid equilibrium restriction.

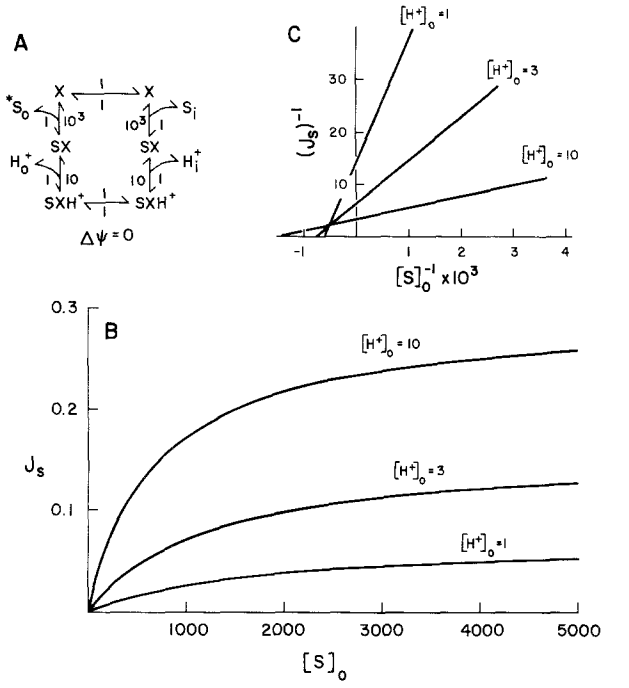

Fig. 7. Increase in both J_{max} and K_m with $[H^+]_o$. (*A*): "FL+" model at equilibrium, with reaction constants shown according to criteria in text and Table 2. As in Fig. 5, ligand concentrations are assumed to be unity for the equilibrium condition. (*B*): Velocity-concentration plots calculated as in Figs. 3*B* and 5*B*. (*C*): Double reciprocal plots of curves in *B*, demonstrating joint effects on J_{max} and K_m

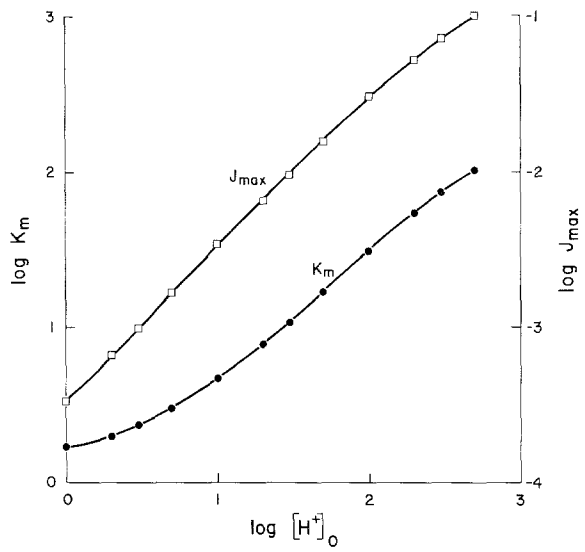

Fig. 8. Joint increase of J_{max} and K_m can hold for more than two orders of magnitude change in $[H^+]_o$. Results of calculations from model in Fig. 7*A* are displayed as points; curves are drawn by eye. Note the increasing tendency toward parallelism of effects on J_{max} and K_m as $[H^+]_o$ is raised out of the range 1–10 (*cf.* Fig. 7*C*): this arises as the product $[H^+]_o \cdot k^o_{42}$ significantly exceeds k_{46}, as predicted in Table 2 (Row 1, Column 3)

D. Opposite Changes of K_m and J_{max}

In general, it might be expected that for increasing $[H^+]_o$ to have opposing effects on K_m and J_{max}, the direction of the effects will be to *decrease* K_m and to *increase* J_{max}, otherwise increased driving force would inhibit the flux. This circumstance represents the transition between Case *A* and Case *B* above, and occurs when the $[H^+]_o$-independent term in the denominators of Eqs. (7a) and (8a) ($k_{13}k_{35}k_{56}$) is about the same magnitude as the $[H^+]_o$-dependent expression, while the dissociation constant for extracellular substrate (k_{46}) is large. Because of its transitional nature, this condition should hold only over a narrow range of driver-ion concentration. Similar reasoning from Cases *A* and *B* shows that, for zero transligand, the transition will occur when $[H^+]_o k^o_{42}$ and k_{24} are of the same magnitude, with k_{46} much larger.

For general computation, with zero membrane potential, the transition could be demonstrated by setting k_{46} at 10^3, poising $k_{24} = 10$ at the midrange for $[H^+]_o k^o_{42}$, and setting the

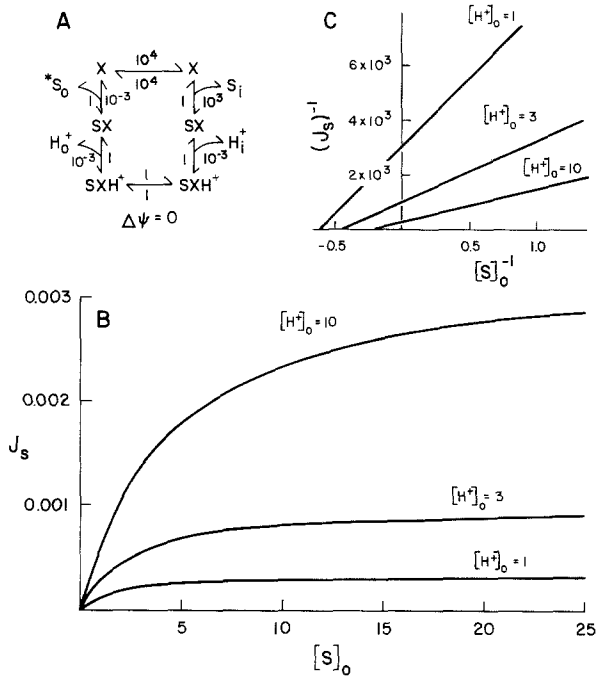

Fig. 9. Opposing effects of $[H^+]_o$ on J_{max} and K_m. (*A*): "FL+" model at equilibrium with reaction constants ordered according to criteria in text, and ligand concentrations set to unity. (*B*): Velocity-concentration plots at different $[H^+]_o$, calculated as in Figs. 3*B*, 5*B* and 7*B*. (*C*): Double reciprocal plot of curves in *B*

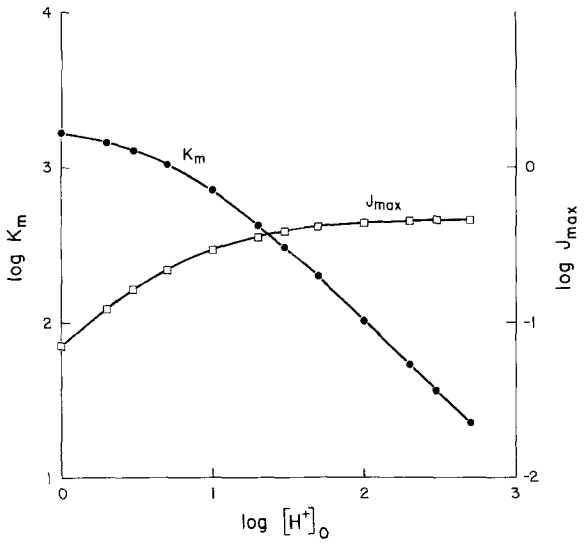

Fig. 10. Relatively restricted range of $[H^+]_o$ over which opposing effects on J_{max} and K_m can be observed. Results of calculations initiated from model in Fig. 9*A* are displayed as points; curves drawn by eye

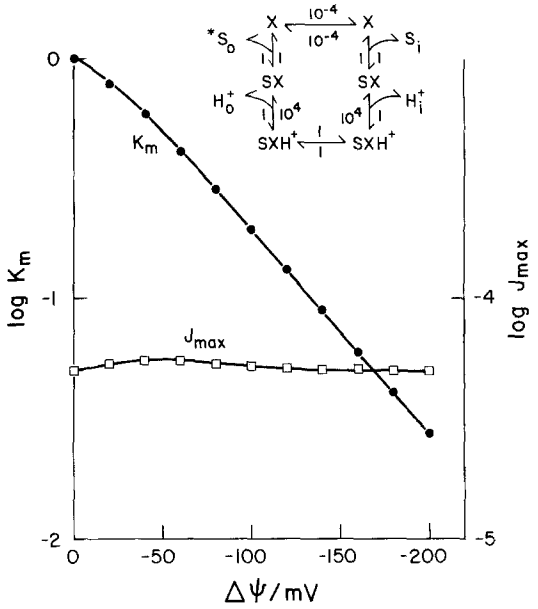

Fig. 11. Selective effect of membrane potential on K_m for transport of S. Figure is plotted to emphasize action of increasingly negative membrane potential as part of the driving force, with the electrochemical gradient of driver ion equal to zero at far left of figure ($[H^+]_o=[H^+]_i=1$, $\Delta\psi=0$). Changes in $\Delta\psi$ were introduced according to Eq. (1). Note dependence of K_m on $\Delta\psi$ is 10-fold/118 mV, as predicted by Eq. (10b), in conjunction with the condition in Table 2 (Row 11, Column 2). *Inset:* "FL+" model, poised at equilibrium and used for the calculations in the figure. Values of the reaction constants are shown, in accordance with the conditions described in the text

product $k_{13}k_{35}k_{56}$ at 10^4, as diagrammed in Fig. 9*A*. The resultant curves (Fig. 9*B*) computed from Eqs. (4)-(6), and their double reciprocal plots (Fig. 9*C*), again confirm expectations based on the restricted Eqs. (7a)-(10a). The display of K_m and J_{max} for a 500-fold rise of $[H^+]_o$ is given in Fig. 10, in which the region of really opposing effects is seen to be restricted to about half a log unit either side of 1 (3-30 in concentration units). Note that the limiting slopes of $+1$ (J_{max}) and -1 (K_m) cannot occur simultaneously at any given $[H^+]_o$.

II. Selective Effects of Membrane Potential on the Kinetic Constants

Since fundamentally similar conclusions — from similar arguments — can be reached about voltage effects on substrate transport, there is no need to redevelop the cases for changing membrane potential. The required conditions are listed in rows 11 and 19 of Table 2, for the "FL+" model. A couple of diagrams may be useful, however, to reinforce the idea that changing membrane potential can, indeed, affect selectively either the K_m or the J_{max} for substrate transport without resort to "allosterism" or other *ad hoc* assumptions.

Consideration of Eqs. (9b), (10b), (11a), and (12a) reveals that increasingly negative membrane potential should selectively reduce the K_m for substrate influx when $k_{24} > k^o_{21}\exp(-u/2) \gg k_{56}$. When, in addition, dissociation of driver ion at the cytoplasmic surface of the membrane is rapid (k_{13} large), the slope of log (K_m) versus membrane potential approaches 1 (10-fold in concentration units) per -118 mV, as dictated by $-u/2$ ($=-F\Delta\psi/2RT$) in the exponential term. These features are demonstrated in Fig. 11. [It should be noted that the condition in which k_{24} and k_{13} are large is the same which was shown earlier to yield *kinetic* interchangeability of the transmembrane differences of membrane potential and H^+ concentration (Hansen et al., 1981).]

The requirements for changes of membrane potential to affect J_{max} selectively are that $k^o_{12}\exp(u/2) > k_{13} \gg k^o_{21}\exp(-u/2)$, which could be taken to mean that at ordinary membrane potentials the preferred direction of the charge-transit step (taken alone) would be outward, contrary to the "forward" transport direction. The limiting slope for $\log(J_{max})$ versus membrane potential is 1 (10-fold in velocity) per -59 mV, twice as steep as for the K_m-relationship discussed above. This arises because k_{21} terms drop out of the denominator, leaving J_{max} proportional to $k^o_{21}\exp(-u/2)/k^o_{12}\exp(u/2)$, so the final expression contains $\exp(-u)$. One example of the selective,

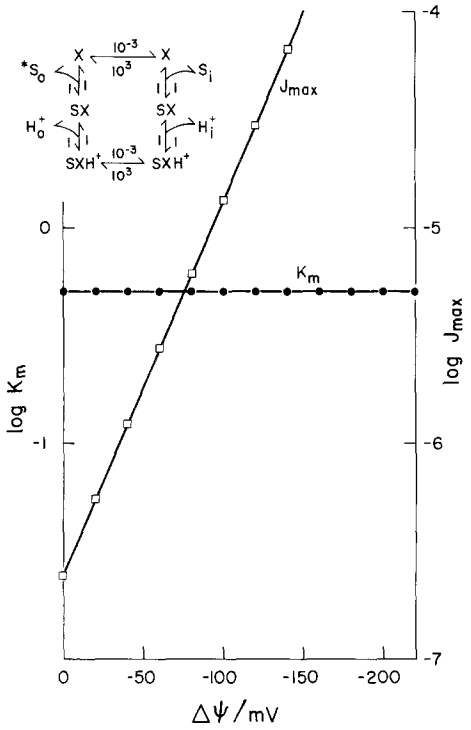

Fig. 12. Selective effect of membrane potential on J_{max}. As in Fig. 11, electrochemical gradient of driver ion is zero at far left of figure. Note dependence of J_{max} on $\Delta\psi$ is 10-fold/59 mV, as predicted by Eq. (9b) and the condition given in Table 2, Row 11, Column 1. *Inset:* "FL+" model, poised at equilibrium, showing the values of the reaction constants used for the calculations in the figure

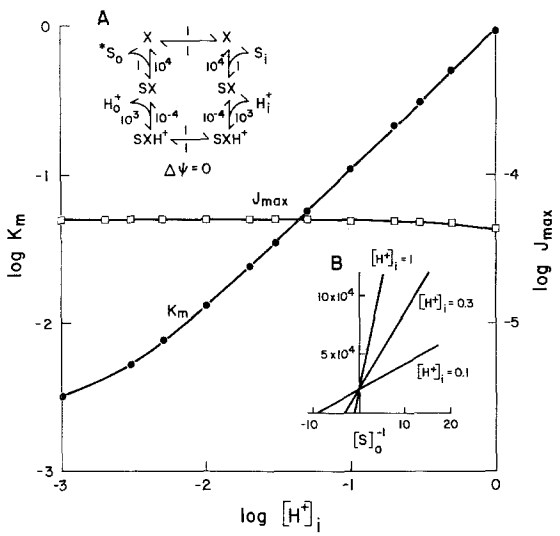

Fig. 13. Selective effect of internal (trans) driver ion concentration ($[H^+]_i$) on K_m of transport of S: competitive inhibition. Electrochemical gradient of driver ion is zero at far right of figure, so the rest of figure reflects net inward gradient. The log-log plot shows selective effects holding over at least three orders of magnitude of $[H^+]_i$, with a maximum slope of K_m approaching 1 (direct proportionality), as predicted by Eq. (8b) in conjunction with condition in Table 2, Row 5, Column 2. *Inset A:* "FL+" model used to generate the figure. Values of the reaction constants are displayed and ordered as discussed in the text, for the equilibrium condition with all ligand concentrations taken as unity. For the calculations, $\Delta\psi$ was set to zero, and N to 1. $[H^+]_i$ was adjusted by variation of k_{31}, as in Fig. 2. *Inset B:* Double reciprocal plot at three different $[H^+]_i$, emphasizing the competitive nature of the inhibition

linear dependence of J_{max} on $\Delta\psi$ is given in Fig. 12.

III. Selective Effects of Intracellular Driver Ion

In experiments with whole cells it is rarely possible to vary the intracellular driver-ion concentration at will, although with large cells perfusion techniques have succeeded for analysis of some co- or counter-transport systems (Requena, 1978; Sanders & Hansen, 1981). On the other hand, by means of reversibly permeablized cells or vesiculated membrane fragments, it is now becoming possible to vary both internal and external substrate and driver-ion concentrations. Emerging technology thus provides a practical justification for exploring the theoretical relationships between intracellular driver-ion concentration and the kinetic parameters for substrate influx.

We have already stated that proper ordering of reaction constants in the transport cycle can yield selective K_m-effects, selective J_{max}-effects, or mixed effects, in response to changing $[H^+]_i$; and the required conditions are summarized in rows 5 and 15 of Table 2 ("FL+" model). The actual results, however, are considerably more interesting than a simple paraphrasing of the behavior with varied $[H^+]_o$, because changes of $[H^+]_i$ can very closely mimic conventional enzyme inhibitor kinetics. That is, rising $[H^+]_i$ can *increase* the K_m for substrate influx (competitive inhibition), or *decrease* the J_{max} (simple linear noncompetitive inhibition). These features are represented in Fig. 13 for an almost pure K_m-effect, and in Fig. 14 for a pure J_{max}-effect.

Inspection of Eqs. (7b), (8b), (11b), and (12b) reveals the condition for generating an almost pure effect of $[H^+]_i$ on the substrate K_m to be $k_{35} > k^o_{31}[H^+]_i \gg k_{13}$. But in this case $[H^+]_i$ survives in the numerator of K_m, not the denominator [Eqs. (8b) and (12b)], making K_m directly proportional to $[H^+]_i$. For the reaction constants chosen (Fig. 13, upper inset), proportionality once again holds over a 100-fold concentration range. A double reciprocal plot (Fig. 13, lower inset) emphasizes the similarity with

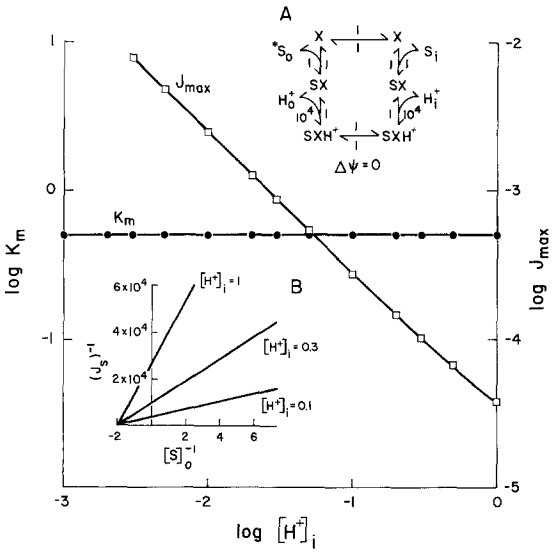

Fig. 14. Selective effect of $[H^+]_i$ on J_{max}: simple linear noncompetitive inhibition. As in Fig. 13, electrochemical gradient for driver ion is zero at far right of figure. Log-log plot shows selective effect on J_{max} holds over three orders of magnitude of $[H^+]_i$, with no detectable effect on K_m. Note linear decline of log (J_{max}) with increasing log ($[H^+]_i$), slope approaching -1, in accordance with the predictions of Eq. (8b) in conjunction with the condition in Table 2, Row 5, Column 1. *Inset A:* "FL+" model, poised at equilibrium, with values of the reaction constants displayed and ordered as discussed in the text: all ligand concentrations taken as unity for this starting condition. Calculations performed as described for Fig. 13. *Inset B:* Double reciprocal plot at three different $[H^+]_i$, displaying simple linear noncompetitive inhibition

conventional competitive inhibition, in that rising $[H^+]_i$ increases the slope without changing the ordinate intercept. [Although data for competitive inhibition are not ordinarily displayed in such a fashion, the similarity also carries over to the log-log plots. Thus, for a simple enzyme with one substrate and one competitive inhibitor, $K'_m = K_m(1+[I]/K_I)$, where K'_m is the apparent Michaelis constant in the presence of inhibitor, $[I]$ is the inhibitor concentration, and K_I is the inhibitor binding constant. When $[I]/K_I \gg 1$, $K'_m \simeq K_m \cdot [I]/K_I$, which is linear with unit slope in a log-log plot.]

The condition for generating a pure J_{max}-effect with changing $[H^+]_i$ is $k^o_{31}[H^+]_i > k_{13}, k_{35}$. Appropriate values of reaction constants are shown in Fig. 14 (upper inset), along with the nearly straight-line plot of J_{max} and constant value of K_m calculated via Eqs. (4)–(6). The double reciprocal plot (lower inset) emphasizes the similarity to conventional noncompetitive inhibition.

The results shown in Figs. 13 and 14 thus make clear that "competitive" or "noncompetitive" inhibition which might be displayed between substrate and trans driver ion in cotransport systems can be explained utterly without reference to such devices as multiple (H^+) binding sites or direct interference (by $[H^+]$) with substrate binding. Table 2 lists the conditions for which uncompetitive inhibition (column 3) and mixed (linear noncompetitive) inhibition (column 4) can also be generated.

IV. Impact of the Equilibrium-Binding Assumption on Model Behavior

The full rate-equations describing model behavior (Eqs. (4)–(6), and Table 1) can easily be simplified according to the classical assumption of equilibrium binding by making all transmembrane reaction constants small. When this is done, much of the flexibility of the model is lost, and we can expect certain classes of experimental data to fall outside the restricted range of the new equations, even though the data are still described by the full rate-equations.

A clear-cut and important case in point is that of $H^+ - SO_4^=$ cotransport in *Penicillium*, as described by Cuppoletti and Segel (1975*b*). [The system might also transport Ca^{2+}, which would assist in energizing $SO_4^=$ accumulation (Cuppoletti & Segel, 1975*a*).] To see the restrictive effect of assuming equilibrium binding, we make the four reaction constants k_{12}, k_{21}, k_{56}, and k_{65} small in Eq. (5), and drop all terms which contain the product of two of these reaction constants. Since the effects of membrane potential and intracellular ligands are not explicitly considered, behavior of Eq. (5) is the same for all models in which S binds before H^+: "FL+", "FL−", "FF+" and "FF−" models. J_{max} for influx of S (sulfate) becomes

$$\frac{J_{max}}{N} = \frac{[H^+]_o k^o_{42} k_{21} F}{[H^+]_o k^o_{42}(F + k_{21}[k_{53}(k_{13}+k_{31}) + k_{13}k_{35}]) + k_{24}F} \quad (13)$$

where $F = k_{13}k_{35}k_{56} + k_{53}k_{31}k_{12}$, and the equation is written specifically to show the effect of external driver-ion concentration on J_{max}. From this equation it can be seen that the overall form of response is a rectangular hyperbola, and that the condition for a simple pro-

portional response of J_{max} to $[H^+]_o$ is that k_{24} be large with respect to $[H^+]_o k^o_{42}$.

By contrast, for all models in which S binds after H^+ ("LL+", "LL−", "LF+", and "LF−"), the same treatment for equilibrium binding leads to

$$\frac{J_{max}}{N} = \frac{k_{21} F}{k_{21} k_{13}(k_{35}+k_{53}) + k_{53} k_{31} k_{21} + F}. \quad (14)$$

Here, J_{max} is completely insensitive to $[H^+]_o$. Therefore, to account for the experimental observation that J_{max} for sulfate uptake by *Penicillium* is insensitive to extracellular pH, Cuppoletti and Segel (1975*b*) concluded cautiously that H^+ must bind first, followed by $SO_4^=$.

Equations (13) and (14) are general ones, expressing J_{max} with respect to the ligand binding first [Eq. (13)] or second [Eq. (14)]. Thus, they can also be applied to cases in which J_{max} is determined for H^+ transport, i.e., J^H_{max}, provided that the ligand identities of the binding terms are switched (e.g., in Eq. (13) k_{42} would incorporate $[S]_o$). This means that J^H_{max} is sensitive to $[S]_o$ when S binds second, but not when S binds first. In fact, Cuppoletti and Segel observed a proportionality between J^H_{max} and $[SO_4^=]_o$, which they argued provided stronger evidence for the binding order H^+ first, $SO_4^=$ second.

Now, inspection of Table 2 (column 2), derived from the complete rate equations, shows a multiplicity of conditions (rows 1–4, 9, 10) under which J_{max} for substrate influx is *insensitive* to $[H^+]_o$, including first-on models, last-on models, and models with charged carriers of either sign. Study of Table 2 (column 4) and Fig. 10 would yield more conditions. More importantly, J_{max} can be *sensitive* to $[H^+]_o$, even for models in which substrate binds last (Table 2, columns 1, 3 and 4). In other words, the implied order of ligand binding which emerges by comparing experimental data with Eqs. (13) and (14) rests *wholly* upon the assumption of equilibrium binding. Given such a conclusion, independent experimental evidence for equilibrium binding would seem to be an essential prerequisite for applying the mathematical condition in kinetic analyses.

V. Experimental Applications

So far, emphasis has been laid on the concept that the diverse kinetic behavior of cotransport systems can be model-independent, relating simply to the relative magnitudes of various reaction constants in the transport cycle. However, since almost any characteristic of cotransport within the confines of Michaelis-Menten kinetics can be accommodated by a very simple framework, the experimentalist is faced with the question of whether particular kinetic data will admit *any* solid interpretation about transport mechanisms. The following account illustrates how at least two types of question can be approached: the order of binding to the carrier, for solute and driver ion; and the magnitude of certain key reaction constants.

A. Binding Order

Only minimal simplifying assumptions were imposed in the derivations (above), so that we could describe the complete rate equations. In many practical cases, however, much further simplification is possible, and then often the behavior of the model becomes dependent on binding order. [The best preparations for studying the order of ligand binding and release are those providing easy, direct control of solution compositions on both sides of the membrane: e.g., internally perfused squid giant axons, the characean algae, resealed erythrocyte ghosts, and isolated membrane vesicles.] A useful application of such simplified experimental conditions is provided by the kinetics of *S (isotopic substrate) influx determined at different intracellular ligand concentrations, while both $\Delta\psi(-)$ and $[H^+]_o$ are saturating. Then variation of $[S]_i$ yields the following equations for the "LL+" model [last on-last off, with charge transfer on the loaded carrier; from Eq. (A18a, b)]:

$$\frac{J_{max}}{N} = \frac{k_{13} k_{35} k_{56}}{[S]_i k^o_{53}(k_{13}+k_{31}) + k_{56}(k_{13}+k_{31}+k_{35}) + k_{13} k_{35}} \quad (15)$$

and

$$K_m = \frac{k_{13} k_{35} k_{56}}{k^o_{42}\{[S]_i k^o_{53}(k_{13}+k_{31}) + k_{56}(k_{13}+k_{31}+k_{35}) + k_{13} k_{35}\}}. \quad (16)$$

Thus J_{max} and K_m *must* respond in parallel to changing $[S]_i$; the ratio J_{max}/K_m is constant; and "slope replots" of double reciprocal plots

Table 3. Specific cotransport responses under restricted experimental conditions[a]

Conditions	Experimental variable	Model[b]							
		FL+	FL−	FF+	FF−	LL+	LL−	LF+	LF−
$[H^+]_o$ saturating $\Delta\psi$ very negative	$[S]_i$	*N*	0	*N*	*U*	*U*	0	*U*	*U*
$[H^+]_o$ saturating $\Delta\psi$ very negative	$[H^+]_i$	*N*	*U*	*N*	0	*U*	*N*	*U*	0
$[H^+]_o$ saturating $\Delta\psi$ very negative $[S]_i=0$	$[H^+]_i$	*U*	*U*	*N*	0	*U*	*N*	*U*	0

[a] *Key*: 0, isotopic flux not sensitive to experimental variable; *U*, *only* uncompetitive inhibition of isotopic influx by the internal ligand; *N*, among other responses, influx can be inhibited in noncompetitive fashion by internal ligand.
[b] Models are designated according to the convention of Fig. 1, for the binding order of substrate and driver ion. "FF," for example, means substrate binds first and is released first in the counter-clockwise operation of the cycles: "first on-first off." The + and − signs indicate that charge transfer is assumed to occur either on the doubly-loaded carrier (+) or on the empty carrier (−).

are $[S]_i$-insensitive. *If any other response is observed, the "LL+" model cannot hold.* Furthermore, since the expressions for J_{max} and K_m are almost identical, internal H^+ (contained in the reaction constant k_{31}) must also be an uncompetitive inhibitor.

A summary of the predicted behavior of the eight different models for these specific conditions is given in Table 3. A third simplifying condition, in addition to saturating $\Delta\psi$ and $[H^+]_o$, is also considered in Table 3: that of variation of $[H^+]_i$ with $[S]_i=0$. **Note** that only one model of the eight can accommodate a selective *decrease* in V_{max} with no effect on K_m as $[H^+]_i$ or $[S]_i$ is raised. In internally perfused *Chara*, both $[H^+]_i$ and $[Cl^-]_i$ act as noncompetitive inhibitors of $2H^+/Cl^-$ cotransport under conditions where $\Delta\psi$ and $[H^+]_o$ strongly favor influx (Sanders & Hansen, 1981). Furthermore, since $[H^+]_i$ is noncompetitive even in the absence of internal Cl^-, the "FF+" model was proposed to account for the data. Table 3 shows that the other models, too, have their own characteristic patterns of response, so that binding order should be determinable. [Equilibrium exchange conditions provide an alternative method of ascertaining binding order. The pattern of activation of substrate transport as driver-ion concentration is increased simultaneously on both sides of the membrane has been shown by Hopfer and Liedtke (1981) to be a useful diagnostic feature.]

B. Evaluation of Specific Reaction Constants

Perhaps the clearest simplifying condition exists when transport is blocked by an inhibitor, making possible direct measurement of the equilibrium dissociation constant (K_D) for substrate, or – better – for a nontransportable analogue (Turner & Silverman, 1980, 1981), although as pointed out by Page and West (1981), transport must be *completely* blocked. But even under less rigorous conditions certain useful relationships can be derived, *as long as binding order is established first.* An excellent example, again, is the case in which $\Delta\psi$ is saturating. [In practice, this condition may generally obtain, at least for proton-coupled systems. Analysis of the current-voltage characteristics of two H^+-cotransport systems, for glucose in *Neurospora* and for amino acids in *Riccia*, have demonstrated marked insensitivity of transport to voltage over a wide range (Hansen & Slayman, 1978; Felle, 1981).] If we take as examples the "FL+" and "FF+" models, Eq. (7a) demonstrates that the effect of a change in $[H^+]_o$ on the J_{max} for transport of *S describes a rectangular hyperbola:

$$\frac{J_{max}}{N}=\frac{J_{stim}[H^+]_o}{K_{stim}+[H^+]_o} \tag{17}$$

with

$$J_{stim}=\frac{k_{13}k_{35}k_{56}}{(k_{13}+k_{31})(k_{53}+k_{56})+k_{35}(k_{13}+k_{56})} \tag{18}$$

and

$$K_{stim}=\frac{k_{13}k_{35}k_{56}}{k^o_{42}[(k_{13}+k_{31})(k_{53}+k_{56})+k_{35}(k_{13}+k_{56})]}. \tag{19}$$

Thus,

$$J_{stim}/K_{stim} = k^o_{42}. \quad (20)$$

Therefore, if N [Eq. (17)] can be estimated by some independent means (e.g., carrier purification or high affinity binding studies), an absolute value can be assigned to the on-reaction constant for H^+_o-binding.

In other cases, the on-reaction constant for *S binding can be determined. For example, with $\Delta\psi$ and $[H^+]_o$ saturating, Eq. (A16a, b) (Table A1) yields, in the cases of "LF+" and "LL+" models, expressions for J_{max} and K_m which are identical with those for J_{stim} and K_{stim} in Eqs. (18), (19). Consequently

$$J_{max}/N \cdot K_m = k^o_{42}. \quad (21)$$

There is an important cautionary note, however: prior determination of binding order in the above example is crucial; the "FL+" and "FF+" models yield more complex expressions for J_{max}/K_m. In other words, not all binding sequences will permit determination of k^o_{42} under a given set of simplifying conditions.

Simple relationships can also emerge from considering the effects on $\Delta\psi$ on J_{max} and K_m. If the experimenter finds a selective effect of $\Delta\psi$ on K_m, for zero trans-ligand conditions (and if charge transfer is assumed to occur on the loaded carrier), then the inequality

$$(k^o_{12} e^{u/2} \text{ or } k_{24}) > (k^o_{21} e^{-u/2} \text{ or } k_{13}) \gg (k_{56} \text{ or } k_{35}) \quad (22)$$

specifies six possible size-orderings of reaction constants (one of which is listed in Table 2: column 2, lines 11–12). For *any* of the four binding orders, J_{max}/N is then usually given simply as k_{56} or k_{35}, whichever is rate limiting.

These conditions for a selective effect of $\Delta\psi$ on K_m represent simple *rate-limitation of transport by carrier recycling*, which in turn implies that the transport system should exhibit counter-flow or exchange diffusion. In fact, the major effect of $\Delta\psi$ on lactose transport in *E. coli* is to reduce the K_m for transport (Overath & Wright, 1980), and the lac carrier system does indeed exhibit marked exchange diffusion (Kaczorowski et al., 1980). [Similar conclusions are obtainable for models in which charge transfer occurs on the unloaded form of the carrier (as is favored by some authors: Kaczorowski et al., 1980), though there the coupling of a selective effect of $\Delta\psi$ on K_m with dominant exchange diffusion is not a unique condition (*see* Table 2: column 2, lines 9–10).]

C. Interaction of Driving Forces; Interpretation of the Proton Well

Reaction kinetic models predict interaction not only between substrate and either of the driving forces – the concentration gradient for the driver ion, or the membrane potential – but also between the two driving forces themselves, even though each acts at a discrete site. Thus, just as membrane potential can cause a selective increase in apparent affinity for transport of substrate (Figs. 3 and 4), so it can also increase the apparent carrier affinity for the driver ion. The necessary orderings of reaction constants can be picked from Table 2, since the requirements for an effect of $\Delta\psi$ on the apparent affinity for the substrate in models where substrate binds first will be similar to those for an effect of $\Delta\psi$ on apparent driver-ion affinity in models with driver-ion binding first. In the "FF+" model, for example, the following condition must hold:

$$k_{24} > k^o_{21} \exp(-u/2) > k_{56}. \quad (23)$$

(*See* Table 2, Row 12, Column 2.) A similar condition was derived differently in an earlier paper (Hansen et al., 1981) and was shown to account for observable equivalence of the electrical and osmotic components of driving force acting on net flux (current).

Increasingly negative membrane potential has indeed been shown to increase the apparent transport affinity for driver ions, as in the case of H^+/glucose cotransport in *Chlorella* (Schwab & Komor, 1978; shown here in the data plots of Fig. 15*B*). The apparent pK of the carrier was reported to shift from 7.01 at −74 mV to 7.54 at −135 mV, although sugar flux at the optimum pH was voltage-insensitive. Taking Eq. (23) as a starting point, we have fitted the data with a straightforward "FF+" model (Fig. 15*A*). The sole effect of external pH on the carrier was assumed to be to increase the rate of the H^+-binding reaction in direct proportion to $[H^+]_o$, and the only effect of membrane potential was on transmembrane transfer of the loaded carrier. [In generating the fitted curves, we have also taken account of the observation that internal pH shows a clear, though weak, dependence on external pH (Komor & Tanner, 1974), and that sugar flux varies as a function of internal pH (Komor, Schwab & Tanner, 1979).] Visually satisfactory fits result –

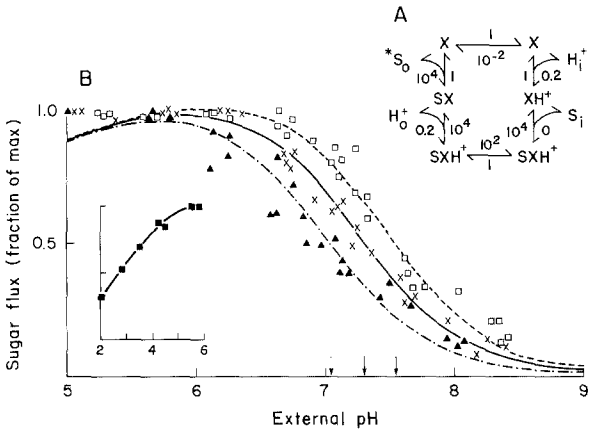

Fig. 15. Apparent change in affinity of driver ion elicited by membrane potential. (*A*): Reaction kinetic model based on Eq. (23) and used to generate the fits in *B*. Values for each of the reaction constants are shown for the condition of no membrane potential and pH = 7 on both sides of the membrane. $\Delta\psi$ introduced according to Eq. (1). Changes in external $[H^+]$ reflected by an equivalent change in k_{42} (*see* Fig. 2*A*) and the concomitant change in internal $[H^+]$ (k_{53} adjusted) was given by the empirical relation of Komor and Tanner (1974):

$$pH_i = 0.31\,pH_o + 5.17$$

k_{31} was set to zero in accordance with the condition that the cells had insignificant internal hexose. (*B*): Data of Schwab and Komor (1978) replotted, with fits generated by model in *A*. Flux of 6-deoxyglucose was measured at three different membrane potentials and over a range of external pH. (▲)·-·-·(▲): −74 mV; (×)——(×): −105 mV; (□)----(□): −135 mV. Maximum flux was independent of $\Delta\psi$. Arrows on abscissa show the pH at which flux is 0.5 of maximum (≡apparent pK) for each of the three curves; values are 7.04 (−74 mV), 7.30 (−105 mV), 7.54 (−135 mV). *Inset:* Decline of flux below pH 6, redrawn from Komor and Tanner (1974). A similar decline is also predicted by the model in *A* due to progressively lowered internal pH

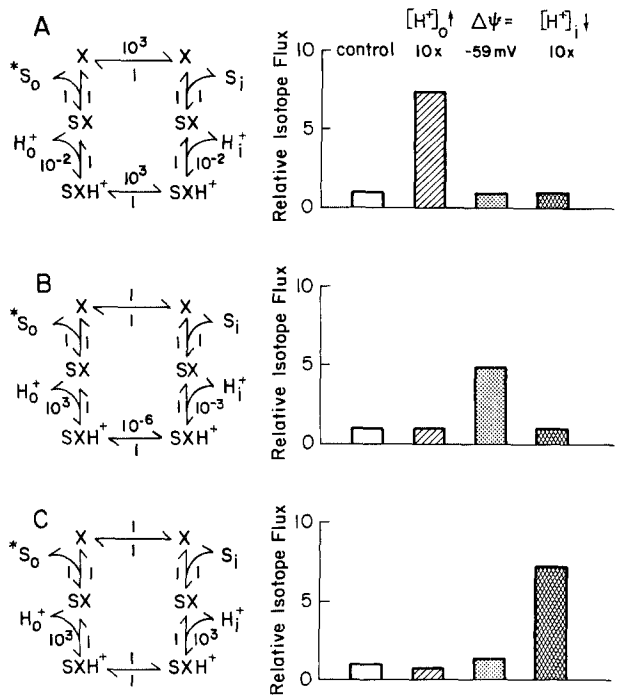

Fig. 16. Nonequivalence of electrical and osmotic components of driver-ion gradient in eliciting transport. In each of models *A*, *B*, and *C*, values of the constants used for calculation of fluxes are shown. All models as drawn are poised at equilibrium. Driving force of −59 mV is introduced in one of three ways: increase of external H^+ binding reaction tenfold; applied $\Delta\psi = -59$ mV, according to Eq. (1); decrease of internal H^+ binding reaction tenfold. Histograms give isotope flux relative to the control for each model

including the predicted shift in apparent pK – without any additional nonspecific effects of external pH or any gating effects of membrane potential. Thus, it is not necessary to invoke a so-called proton well (which also could serve to transduce the electrical potential into a proton gradient) as an explanation for the interaction between the two components of driving force (*cf.* Mitchell, 1969; Mitchell & Moyle, 1974; Komor & Tanner, 1980; Maloney, 1982).

D. Saturation of Driving Forces, and Stoichiometry Changes

A complementary circumstance to that discussed above is the case in which one component of the driving force is saturated, but the other is not. This situation has already been implicitly dealt with in Eqs. (7) through (12), but we return to it here in order to emphasize the important point that substrate flux can depend not upon the driving force *per se*, but on the manner in which the driving force is applied. Figure 16 shows three cotransport systems poised at equilibrium prior to the experiment (control). (These models do not contain any particularly unlikely features. For example, the carrier in Fig. 16*A* can be described simply as having a low pK and a marked passive tendency to reside at the inner surface of the membrane.) A driving force equivalent to −59 mV is then imposed across each model in one of three ways: by raising $[H^+]_o$ 10-fold, by adding a membrane potential of −59 mV, or by lowering $[H^+]_i$ 10-fold. Clearly, only one of the three treatments elicits an enhanced flux, and this treatment is different in each case. Qualitatively, it can be stated that for each model only one accessible reaction constant rate-limits transport, and unless that limitation is lifted trans-

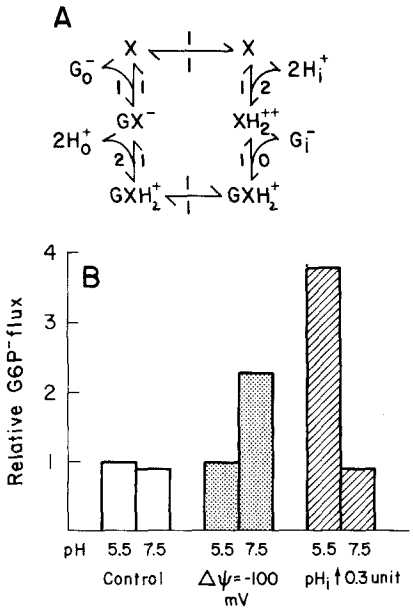

Fig. 17. Simulation of glucose-6-phosphate ($G6P^-$) flux in *E. coli* membrane vesicles (Le Blanc et al., 1980) showing that efficacy of chemical and electrical components of driver ion gradient in driving transport depends on driver ion concentration. (*A*): Reaction kinetic model for $2H^+$:$G6P^-$ cotransport. All reaction constants were initially set equal to 1, with exception of the following: $k_{31}=0$, since no $G6P^-$ was inside vesicles at start of experiment; $k_{42}=k_{53}=2$ at pH 6.5. k_{42} and k_{53} were changed as the square of the $[H^+]$, since $2H^+$ were assumed to bind. (*B*): Fluxes predicted by the model at the two pH's used by Le Blanc et al. and for their conditions (listed on the abscissa). The amount by which intravesicular pH was raised (right hand experiment) was uncertain - an arbitary value of 0.3 unit has been used here. Left and center experiments: $k_{42}=k_{53}$. $\Delta\psi$ introduced in center experiment according to Eq. (1)

port cannot be stimulated by imposing a driving force in other ways.

An important corollary of this result is that insensitivity of transport to variation of one component of the driving force is not evidence against the involvement of that component in transport. In particular, voltage-insensitivity does not necessarily indicate that transport is electroneutral. LeBlanc, Rimon and Kaback (1980) demonstrated that glucose-6-phosphate ($G6P^-$) transport in *E. coli* membrane vesicles is much more potential-sensitive at pH 7.5 than at pH 5.5, but that a pH gradient is more effective in driving transport at the lower pH. Their conclusion that transport is electroneutral at the lower pH but electrogenic at higher pH - and hence that H^+:$G6P^-$ stoichiometry changes as a function of pH - although also consistent with the data, is simply not necessary. [This point has also been made in connection with similar data by Booth et al. (1979).] The data also permit transport to be rate-limited by intravesicular pH at pH 5.5 and by membrane potential at pH 7.5. The overall effect is modelled in Fig. 17 for *constant* H^+:$G6P^-$ stoichiometry (=2).

Discussion

General Conclusions

The long-standing notion that carrier-mediated transport is rate limited at the translocation steps seems to have had three origins. The first, a conviction that large, intramembrane proteins would behave as relatively immobile structures, alternating their orientation only slowly, can now be replaced by the view that translocation involves only *intra*molecular, or conformational, changes in the carrier, not gross rearrangement. There is reason to believe that these conformational changes could occur at least as fast as the ligand binding reactions. For example, in kidney brush border vesicles, Na^+ dissociation from the Na^+/glucose cotransport system occurs at only 10–20% of the rate for membrane transit (Hopfer & Groseclose, 1980; *see also* Crane & Dorando, 1980). Even where carrier-mediated transport involves transmembrane diffusion of the whole carrier (valinomycin), rate constants for ligand binding and for translocation have been found to be of similar magnitude (Läuger, 1980). Second, the unwieldiness of the complete rate equation for a multistate carrier created a need for mathematical simplification, which was obtained by assuming slow transmembrane reactions and equilibrium binding (Laidler, 1956). Finally, the general success of equilibrium binding treatments in enzyme kinetics educed a belief that carrier systems would obey similar rules.

In the present paper, we have used a different strategy to reduce algebraic complexity: simplify the algebra using *special conditions which are attainable experimentally*, and then compare the behavior of the resulting equations with that of the complete model, by numerical methods. In all cases, good qualitative agreement has been found, and several major conclusions have emerged from the analysis, each having important implications for interpretation of experimental data.

Most importantly, it is clear that even the simplest kinetic model for cotransport can generate a diverse range of gross kinetic effects whose exact form is merely a function of the relative values of the carrier reaction constants. Thus, dramatic differences in the kinetic characteristics of individual transport systems cannot necessarily be taken as evidence for different sites of action of an applied ligand – a point which was initially recognized by Rosenberg and Wilbrandt (1955). It follows, therefore, that the particular kinetic effect exerted by one ligand (cis *or* trans to the side from which transport is measured) or by membrane potential, if considered alone, yields little solid insight into the mechanism of transport.

The above conclusion is in direct contrast to that of Heinz et al. (1972) and Geck and Heinz (1976), who assumed equilibrium binding and special sites of action of driving force on the carrier. There, specific effects of driver-ion concentration or membrane potential on gross kinetic constants were used to determine the mechanism of energy coupling. Two types of model were considered: an "affinity" type, in which the driver ion modified only the affinity of the carrier for the substrate, and a "velocity" type, in which the driver ion selectively increased carrier mobility. In either case, the driver ion produced changes in carrier behavior which require ad hoc adjustments of the model. Many authors have commented on the possibility of applying affinity or velocity models to their data (e.g., Schwab & Komor, 1978; Overath & Wright, 1980; West, 1980). However, since straightforward kinetic models – in which the actions of driver ion and membrane potential are strictly defined by Eqs. (1) and (2), and the legend of Fig. 2 – can explain these diverse responses, there is no reason to invoke less well-defined explanations. [In some cases, indeed, neither velocity models nor affinity models can adequately explain the data. An example is provided by the effect of membrane potential on the *lac* carrier in *E. coli*. Imposition of a negative membrane potential on vesicles lowers K_m by two orders of magnitude, but has no effect on J_{max} (Overath & Wright, 1980); but both affinity and velocity *models* require that J_{max}, as well as K_m, increase as membrane potential becomes more negative (Geck & Heinz, 1976). Figure 11 in the present paper gives the required result straight from the model of Fig. 1 (conditions in Table 2: column 2, lines 11–12).]

A second conclusion of the present work is that, although diverse kinetic effects of ligands or membrane potential are obtainable for any particular reaction kinetic model, it may nevertheless be possible to determine ligand binding order, site of charge transfer, and even individual reaction constants, by careful choice of experimental conditions.

The third, and most general, conclusion has been drawn previously by us (Hansen et al., 1981) and by Chapman, Johnson and Kootsey (1983) with respect to the current-voltage relations of electrogenic pumps, but is reiterated here in the context of isotope fluxes. There has been a strong tendency, stimulated by the general success of irreversible thermodynamics, to view flux and force as strictly proportional, and independent of the form (electrical or osmotic) which the driving force takes. Yet, as Fig. 16 illustrates for simple kinetic models, driving forces of different nature but the same magnitude can easily generate different transport responses, *even in the vicinity of equilibrium*. Moreover, just as the occurrence of Michaelis-Menten kinetics implies saturability of the flux with respect to solute chemical gradients, so the equations governing the response of flux to other components of driving force predict saturability. While the magnitude of the prevailing electrochemical gradient must determine the equilibrium concentrations on each side of the membrane (providing there are no leaks), it cannot be used to predict kinetics without other information on the characteristics of the carrier. It is interesting to note that in some instances an isotopic flux can even respond paradoxically to an imposed driving force. An example is given in Fig. 16, Model *C*, where a 10-fold increase in the external driver-ion concentration decreases the isotope flux by 20% (though net flux or current will show a small increment, in accordance with thermodynamic considerations). The response of the isotopic flux in this case can be viewed as inhibition of exchange diffusion.

Testing the Reaction Kinetic Approach; Development of Further Models

While the range of applicability of the simple reaction kinetic analysis is very wide, it is nevertheless clear that certain experimental data will fall outside it. The question then arises as to what kinds of extensions are reasonable, still within the general confines of our approach. One important extension is that of random

binding for substrate and driver ion. Random binding might be expected for solutes showing biphasic kinetics (biphasic activation curves; Segel, 1975) as is the case for many plant and microbial transport systems which appear to be gradient-driven (Epstein, 1976). Schwert (1954) has pointed out that in many cases random-binding reactions will exhibit Michaelis-Menten kinetics, although this would appear to require that over the operational range one binding order is favored, or that the binding constants of ligands to different carrier states happen to be identical. Evidence for random binding is best gathered from equilibrium exchange studies (Hopfer & Liedtke, 1981).

Another simple extension is to suppose that the binary substrate-carrier complex is permeant. The carrier could then be said to possess an internal leak or "slip." The concept of slip reactions has been strongly espoused by Eddy (1980; 1982) as an explanation for the decrease in accumulation ratios of gradient-coupled solutes at high extracellular solute concentrations. In most cases, however, it will be difficult, unless genetic or reconstitution techniques are used, to distinguish whether such a leak is truly intrinsic to the cotransport system or occurs by a separate pathway. Furthermore, it is also possible that straightforward "tight" reaction kinetic models effectively shut down or "transinhibit" at high internal substrate concentrations, despite the presence of a driving force; the point is discussed further below.

Random binding and slip modifications greatly increase the algebraic complexity of transport rate-equations, both because they introduce additional rate constants and because they involve *branched* pathways. Since we have been able to mimic all major kinetic effects of driver-ion and $\Delta\psi$ with the simple sequential models, we have not analyzed random binding or slip here. However, these modifications are merely additions to the simpler models, so that all kinetic effects possible with the simple models are also possible with these variants. In addition, of course, random binding and slip can describe non-Michaelis-Menten kinetics.

Random binding of H^+ and sulfate to the chloride transporter of erythrocytes has been proposed by Milanick and Gunn (1982). Conversely, Na^+ and glucose bind in ordered fashion to a cotransport system in renal brush border (Hopfer & Groseclose, 1980). Nonetheless, it is important to stress that although the ordered binding models considered in this paper are extremely flexible in their kinetics, random addition of ligands remains a viable alternative.

At present, the apparent kinetic diversity of straightforward reaction kinetic models appears to obviate the need for more elaborate refinements of carrier theory, such as the effects of membrane potential or of membrane surface charge on effective ionic concentration at the carrier site (Mitchell, 1969; Roomans & Borst-Pauwels, 1978).

Possible Physical Interpretations of Ordered Binding

The above brief consideration of random binding raises one additional important issue. Formally, ordered binding is simpler – in the sense of requiring only six carrier states; but mechanistically, random binding is simpler, because any enzyme or carrier with two *independent* ligand-binding sites should be able to form in either order. Then the existence of kinetically ordered binding must imply one of two features for the reaction: (i) The "on" reaction constant for one of the ligands is much faster than for the other. Thus, although each ligand might bind independently (in random order), binding would be *statistically* ordered. (In that case it should be possible to raise the concentration of the slowly bound species sufficiently to shift the apparent binding order.) (ii) Or, binding of one ligand might facilitate binding of the other, either through a conformational change in the carrier molecule or through direct, ligand-ligand interaction. The overall process could be described as *sterically* ordered binding.

Now, on the one hand, statistically ordered binding implies specific size-ordering of (some) reaction constants; and, on the other hand, sterically ordered binding merges philosophically with some of the ad hoc assumptions (*see* Introduction) we have eschewed in this paper. Therefore, in considering the results of Figs. 3–14 as summarized in Table 2, we must assess the extent to which inherent contradictions in statistically ordered binding would force us to fall back on sterically ordered binding.

In fact, problems of this kind need be considered only in relation to substrate and driver-ion *release* at the cytoplasmic face of the membrane. This conclusion follows from the use, not of transport velocity *per se*, but of J_{max} and K_m (for substrate) as the comparison parameters in kinetic analysis. Because (external) substrate

concentration ($[S]_o$) is extracted as the independent variable in Eq. (4), its binding constant ($k^o = k^o_{64}$ or $= k^o_{42}$) does not enter J_{max} at all [Eq. (5)] and enters K_m only as a *scaling factor* [Eq. (6)]. If we consider ligand release, then statistical ordering requires that $k_{13} \gg k_{35}$. Inspection of Table 2 reveals only 4 cases – in columns 2, 4 and rows 5, 15 – which conflict by requiring $k_{35} \gg k_{13}$. Thus, among the various kinetic phenomena which have been described in Figs. (3)–(14), only those involving apparent competitive inhibition by intracellular driver ion, under "LL" and "FL" models (Fig. 13), would require steric ordering.

The Kinetic Effect of Hidden Carrier States

In constructing a minimal model for cotransport, we have assumed that the carrier exists only in six states. But the experimenter can never be sure that all carrier states have been identified; e.g., if ligands were to cross the membrane via a *series* of discrete conformational changes, many carrier states could be hidden. The problem is a general one in enzymology and means that, even if a reaction constant can be measured in theory, there remains the possibility that in reality it consists of more than one elementary rate constant. In an earlier paper (Hansen et al., 1981) we have also discussed how hidden states *elsewhere* in the reaction cycle can affect the apparent values of identified reaction constants, formally taking account of such effects via so-called reserve factors. These factors arise because the *total carrier present in the identified states* is not necessarily constant, as assumed for the derivation of the rate equation [(*see* Eq. (3)]. In Appendix II, we have demonstrated that hidden states do not compromise the basic conclusions of this paper.

Homeostasis: Cytoplasmic Composition and Transport Regulation

The total driving force stored in an ion gradient and imposed across a cotransport system can reach −300 mV (Sanders & Slayman, 1982) – or even higher when the stoichiometric coefficient is taken into account. A free energy gradient of this size should sustain steady state accumulations of solute up to 10^5-fold (as for amino acids in fungi; Eddy, 1978), which might be beneficial to cells bathed in micromolar solute, but is clearly not acceptable if the external concentration lies in the millimolar range. The possibility of selective determination of flux by internal ligands (Fig. 16*C*) suggests that this aspect of kinetics could confer selective advantage on a cell for which control of internal solute concentration is important. This point is made more forcefully in Fig. 18 for a *net* flux: as internal solute concentration rises, net transport (current flow) is steeply inhibited, *despite* the presence of a large driving force. [Figure 18 is a specific demonstration of the finding that transport is not proportional to driving force

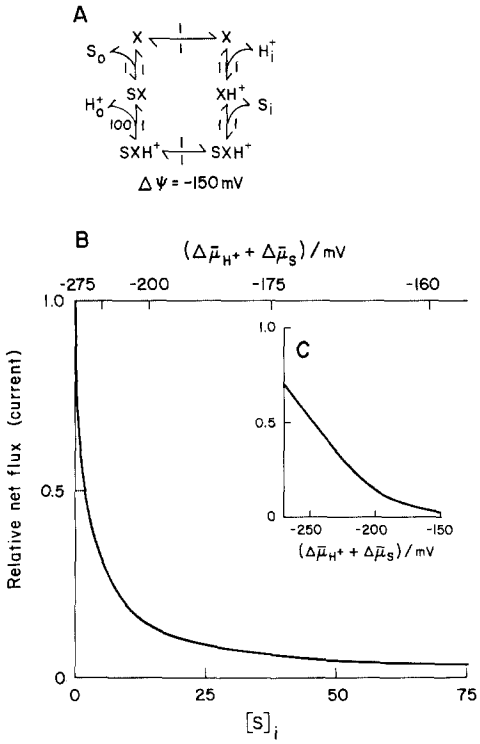

Fig. 18. Transinhibition in the presence of a driving force; apparent ligand-controlled gate. (*A*): Reaction kinetic scheme on which modelling is based. All reaction constants set to 1 except that subsuming binding of external H^+ (=100). Membrane potential set to −150 mV and introduced into reaction constants for transmembrane reactions of loaded carrier as described in Eq. (1). Total driving force across system calculated as sum of electrochemical potential gradients of H^+ ($\Delta\bar{\mu}_{H^+}$) and S ($\Delta\bar{\mu}_S$). Initially, $\Delta\bar{\mu}_{H^+} = -268$ mV and $\Delta\bar{\mu}_S = 0$. The electrical and chemical components of $\Delta\bar{\mu}_{H^+}$ have been assigned values typical for a nonanimal cell (−150 and −118 mV, respectively). (*B*): Effect of increase in internal [S] (appropriate binding constant adjusted accordingly) on net flux of S. Upper scale gives computed driving force as internal [S] increases. (*C*) (Inset): The same data plotted as a function of the driving force on a linear scale. Note the apparent "gating" effect around −150 to −200 mV and the linearity of flux and driving force at larger (absolute) values of the driving force

and is analogous to our earlier demonstration (Hansen et al., 1981) that voltage thresholds resembling gates can occur far from equilibrium for electrogenic transport.] Many examples of this transinhibition are known, especially for amino acids in bacteria and fungi (Ring & Heinz, 1966; Crabeel & Grenson, 1970; Pall, 1971; Kotyk & Rihova, 1972; Morrison & Lichtstein, 1976; *see also* Belkhode & Scholefield, 1969; Russell, 1976; Giaquinta, 1980; Sanders, 1980*a*). Near-cessation of transport at high internal levels of substrate has many of the characteristics of a feedback system, but is more economical since it involves no messengers other than the necessary components of transport (i.e., ligand and carrier). The occurrence of transinhibition demands caution in attempts to measure driver ion/solute stoichiometry from steady-state transmembrane solute gradients: the steady state will not in general represent true equilibrium. It should be noted, finally, that transinhibition provides a simple reaction kinetic explanation for the observation that steady-state accumulation ratios decrease as external solute concentrations rise. It is an attractive and economical alternative to the hypothesis of internal slips (*see* above).

If the relative values of reaction constants have evolved in response to the need for intrinsic regulation of transport, as these arguments suggest, then it comes as no surprise to discover a large diversity of kinetic behavior in cotransport. Each transport system will operate in accord with the specific homeostatic requirements of the cell type in which it is found, and it seems likely that this fact, not differences in *mechanism* of transport, mainly accounts for kinetic diversity.

This work was supported by grant GM-15858 from the National Institute of General Medical Sciences. We thank Drs. P.S. Aronson, E.L. Boulpaep, B. Forbush, S.A. Lewis, M.A. Milanick, and G. Rudnick for critical comments on the manuscript.

References

Aronson, P.S., Sacktor, B. 1975. The Na^+ gradient-dependent transport of D-glucose in renal brush border vesicles. *J. Biol. Chem.* **250**:6032–6039

Belkhode, M.L., Scholefield, P.G. 1969. Interactions between amino acids during transport and exchange diffusion in Novikoff and Ehrlich ascites tumor cells. *Biochim. Biophys. Acta* **173**:290–301

Booth, I.R., Mitchell, W.J., Hamilton, W.A. 1979. Quantitative analysis of proton-linked transport systems: The lactose permease of *Escherichia coli*. *Biochem. J.* **182**:687–696

Boudart, M. 1976. Consistency between kinetics and thermodynamics. *J. Phys. Chem.* **80**:2869–2870

Broek, P.J.A. van den, Steveninck, J. van 1980. Kinetic analysis of simultaneously occurring proton-sorbose symport and passive sorbose transport in *Saccharomyces fragilis*. *Biochim. Biophys. Acta* **602**:419–432

Cha, S. 1968. A simple method for derivation of rate equations for enzyme-catalyzed reactions under the rapid equilibrium assumption or combined assumptions of equilibrium and steady state. *J. Biol. Chem.* **243**:820–825

Chapman, J.B. 1982. A kinetic interpretation of "variable" stoichiometry for an electrogenic sodium pump obeying chemiosmotic principles. *J. Theor. Biol.* **95**:665–678

Chapman, J.B., Johnson, E.A., Kootsey, J.M. 1983. Electrical and biochemical properties of an enzyme model of the sodium pump. *J. Membrane Biol.* **74**:139–153

Cleland, W.W. 1967. Enzyme kinetics. *Annu. Rev. Biochem.* **36**:77–112

Cohen, S.R. 1980. The complete rate equation, including the explicit dependence on Na^+ ions, for the influx of α-aminoisobutyric acid into mouse brain slices. *J. Membrane Biol.* **52**:95–105

Crabeel, M., Grenson, M. 1970. Regulation of histidine uptake by specific feedback inhibition of two histidine permeases. *Eur. J. Biochem.* **14**:197–204

Crane, R.K., Dorando, F.C. 1980. On the mechanism of Na^+-dependent glucose transport. *Ann. N.Y. Acad. Sci.* **339**:46–52

Crane, R.K., Miller, D., Bihler, I. 1961. The restrictions on possible mechanisms of intestinal active transport of sugars. *In:* Membrane Transport and Metabolism. A Kleinzeller and A. Kotyk, editors. pp. 439–449. Academic Press, London

Cuppoletti, J., Segel, I.H. 1975*a*. Kinetics of sulfate transport by *Penicillium notatum*. Interactions of sulfate, protons, and calcium. Biochemistry **14**:4712–4718

Cuppoletti, J., Segel, I.H. 1975*b*. Kinetic analysis of active membrane transport systems: Equations for net velocity and isotope exchange. *J. Theor. Biol.* **53**:125–144

Curran, P.F., Schultz, S.G., Chez, R.A., Fuisz, R.E. 1967. Kinetic relations of the Na^+-amino acid interaction at the mucosal border in intestine. *J. Gen. Physiol.* **50**:1261–1286

Delrot, S., Bonnemain, J.L. 1981. Involvement of protons as a substrate for the sucrose carrier during phloem loading in *Vicia faba* leaves. *Plant Physiol.* **67**:560–564

Despeghel, J.-P., Delrot, S. 1983. Energetics of amino acid uptake by *Vicia faba* leaf tissues. *Plant Physiol.* **71**:1–6

Eddy, A.A. 1978. Proton-dependent solute transport in microorganisms. *In:* Current Topics in Membranes and Transport. F. Bronner and A. Kleinzeller, editors. Vol. 10, pp. 279–360. Academic Press, New York

Eddy, A.A. 1980. Slip and leak models of gradient-coupled transport. *Trans. Biochem. Soc. London* **8**:271–273

Eddy, A.A. 1982. Mechanisms of solute transport in selected eucaryotic microorganisms. *Adv. Microb. Physiol.* **23**:1–78

Eddy, A.A., Mulcahy, M.F., Thomson, P.J. 1967. The effects of sodium ions and potassium ions on glycine uptake by mouse ascites tumour cells in the presence and absence of selected metabolic inhibitors. *Biochem. J.* **103**:863–876

Epstein, E. 1976. Kinetics of ion transport and the carrier concept. *In:* Encyclopedia of Plant Physiology, Vol 2,

Part B. Tissues and Organs. M.G. Pitman and U. Lüttge, editors. pp. 70–94. Springer-Verlag, Berlin

Felle, H. 1981. Stereospecificity and electrogenicity of amino acid transport in *Riccia fluitans*. *Planta* **152**:505–512

Geck, P., Heinz, E. 1976. Coupling in secondary transport. Effect of electrical potentials on the kinetics of ion-linked cotransport. *Biochim. Biophys. Acta* **443**:49–53

Geck, P., Heinz, E. 1978. The electrical potential difference as a driving force in Na^+-linked cotransport of organic solutes. *In:* Membrane Transport Processes. Vol. 1. J.F. Hoffman, editor. pp. 13–30. Raven Press, New York

Giaquinta, R. 1980. Sucrose/proton cotransport during phloem loading and its possible control by internal sucrose concentration. *In:* Plant Membrane Transport: Current Conceptual Issues. R.M. Spanswick, W.J. Lucas, and J. Dainty, editors. pp. 273–282. Elsevier, Amsterdam

Goldner, A., Schultz, S.G., Curran, P.F. 1969. Sodium and sugar fluxes across the mucosal border of rabbit ileum. *J. Gen. Physiol.* **53**:362–383

Gradmann, D., Hansen, U.-P., Slayman, C.L. 1982. Reaction-kinetic analysis of current-voltage relationships for electrogenic pumps in *Neurospora* and *Acetabularia*. *In:* Current Topics in Membranes and Transport. Vol. 16, pp. 257–281. C.L. Slayman, editor. Academic Press, New York

Hansen, U.-P., Gradmann, D., Sanders, D., Slayman, C.L. 1981. Interpretation of current-voltage relationships for "active" ion transport systems: I. Steady-state reaction-kinetic analysis of class-I mechanisms. *J. Membrane Biol.* **63**:165–190

Hansen, U.-P., Slayman, C.L. 1978. Current-voltage relationships for a clearly electrogenic cotransport system. *In:* Membrane Transport Processes. Vol. 1. J.F. Hoffman, editor. pp. 141–154. Raven Press, New York

Heinz, E., Geck, P., Wilbrandt, W. 1972. Coupling in secondary active transport. Activation of transport by cotransport and/or countertransport with the fluxes of other solutes. *Biochim. Biophys. Acta* **255**:442–461

Hill, T.L. 1977. Free Energy Transduction in Biology. Academic Press, New York

Hill, T.L., Eisenberg, E. 1981. Can energy transduction be localized at some crucial part of the enzymatic cycle? *Q. Rev. Biophys.* **14**:463–511

Hopfer, U. 1977. Kinetics of Na^+-dependent D-glucose transport. *J. Supramol. Struct.* **7**:1–13

Hopfer, U., Groseclose, R. 1980. The mechanism of Na^+-dependent D-glucose transport. *J. Biol. Chem.* **255**:4453–4462

Hopfer, U., Liedtke, C.M. 1981. Kinetic features of cotransport mechanisms under isotope exchange conditions. *Membrane Biochem.* **4**:11–29

Inui, Y., Christensen, H.N. 1966. Discrimination of single transport systems. The Na^+-sensitive transport of neutral amino acids in the Ehrlich cell. *J. Gen. Physiol.* **50**:203–224

Jacquez, J.A. 1972. Models of ion and substrate cotransport and the effect of membrane potential. *Math. Biosci.* **13**:71–93

Kaczorowski, G.J., Robertson, D.E., Garcia, M.L., Padan, E., Patel, L., Le Blanc, G., Kaback, H.R. 1980. Energetics and mechanism of lactose translocation in isolated membrane vesicles of *Escherichia coli*. *Ann. N.Y. Acad. Sci.* **358**:307–321

King, E.L., Altman, C. 1956. A schematic method of deriving the rate laws for enzyme-catalyzed reactions. *J. Phys. Chem.* **60**:1375–1378

Komor, E., Schwab, W.G.W., Tanner, W. 1979. The effect of intracellular pH on the rate of hexose uptake in *Chlorella*. *Biochim. Biophys. Acta* **555**:524–530

Komor, E., Tanner, W. 1974. The hexose-proton cotransport system of *Chlorella*. pH-dependent change in K_m values and translocation constants of the uptake system. *J. Gen. Physiol.* **64**:568–581

Komor, E., Tanner, W. 1980. Proton-cotransport of sugars in plants. *In:* Plant Membrane Transport: Current Conceptual Issues. R.M. Spanswick, W.J. Lucas, and J. Dainty, editors. pp. 247–257. Elsevier, Amsterdam

Kotyk, A., Rihova, L. 1972. Transport of α-aminoisobutyric acid in *Saccharomyces cerevisiae*. *Biochim. Biophys. Acta* **288**:380–389

Laidler, K.J. 1956. General steady state equations in enzyme and other catalysed reactions. *Trans. Faraday Soc.* **52**:1374–1382

Lanyi, J.K. 1978. Coupling of aspartate and serine transport to the transmembrane electrochemical gradient for sodium ions in *Halobacterium halobium*. Translocation stoichiometries and apparent cooperativity. *Biochemistry* **17**:3011–3018

Läuger, P. 1980. Kinetic properties of ion carriers and channels. *J. Membrane Biol.* **57**:163–178

Läuger, P., Stark, G. 1970. Kinetics of carrier-mediated ion transport across lipid bilayer membranes. *Biochim. Biophys. Acta* **211**:458–466

Le Blanc, G., Rimon, G., Kaback, H.R. 1980. Glucose 6-phosphate transport in membrane vesicles isolated from *Escherichia coli:* Effect of imposed electrical potential and pH gradient. *Biochemistry* **19**:2522–2528

Maloney, P.C. 1982. Energy coupling to ATP synthesis by the proton-translocating ATPase. *J. Membrane Biol.* **67**:1–12

Milanick, M.A., Gunn, R.B. 1982. Proton-sulfate co-transport. Mechanism of H^+ and sulfate addition to the chloride transporter of human red blood cells. *J. Gen. Physiol.* **79**:87–113

Mitchell, P. 1963. Molecule, group and electron translocation through natural membranes. *In:* The Structure and Function of Membranes and Surfaces of Cells. D.J. Bell and J.K. Grant, editors. pp. 142–168. Cambridge University Press, London

Mitchell, P. 1969. Chemiosmotic coupling and energy transduction. *Theor. Exptl. Biophys.* **2**:159–216

Mitchell, P., Moyle, J. 1974. The mechanism of proton translocation in proton-translocating adenosine triphosphatases. *Biochem. Soc. Spec. Publ.* **4**:91–111

Mitchell, W.J., Booth, I.R., Hamilton, S.W. 1979. Quantitative analysis of proton-linked transport systems: Glutamate transport in *Streptococcus aureus Biochem. J.* **184**:441–449

Morrison, C.E., Lichtstein, H.C. 1976. Regulation of lysine transport by feedback inhibition in *Saccharomyces cerevisiae*. *J. Bacteriol.* **125**:864–871

Munck, B.G., Schultz, S.G. 1969. Lysine transport across isolated rabbit ileum. *J. Gen. Physiol.* **53**:157–182

Niiya, S., Moriyama, Y., Futai, M., Tsuchiya, T. 1980. Cation coupling to melibiose transport in *Salmonella typhimurium*. *J. Bacteriol.* **144**:192–199

Overath, P., Wright, J.K. 1980. Lactose carrier protein of *Escherichia coli:* Studies on purification, biosynthesis, and mechanism. *Ann. N.Y. Acad. Sci.* **358**:292–306

Page, M.G.P., West, I.C. 1981. The kinetics of the β-

galactoside-proton symport of *Escherichia coli*. *Biochem. J.* **196**:721–731
Pall, M.L. 1971. Amino acid transport in *Neurospora crassa:* IV. Properties and regulation of a methionine transport system. *Biochim. Biophys. Acta* **233**:201–214
Peterson, N.A., Raghupathy, E. 1973. Developmental transitions in uptake of amino acids by synaptosomal fractions isolated from rat cortex. *J. Neurochem.* **21**:97–110
Reeves, J.P., Sutko, J.L. 1980. Sodium-calcium exchange activity generates a current in cardiac membrane vesicles. *Science* **208**:1461–1464
Reich, J.G., Sel'kov, E.E. 1981. Energy Metabolism of the Cell-A Theoretical Treatise. Academic Press, New York
Requena, J. 1978. Calcium efflux from squid axons under constant sodium electrochemical gradient. *J. Gen. Physiol.* **72**:443–470
Ring, K., Heinz, E. 1966. Active amino acid transport in *Streptomyces hydrogenans:* I. Kinetics of uptake of α-aminoisobutyric acid. *Biochem. Z.* **344**:446–461
Roomans, G.M., Borst-Pauwels, G.W.F.H. 1978. Co-transport of anions and neutral solutes with cations cross charged biological membranes. Effects of surface potential on uptake kinetics. *J. Theor. Biol.* **73**:453–468
Rosenberg, T., Wilbrandt, W. 1955. The kinetics of membrane transports involving chemical reactions. *Exp. Cell Res.* **9**:49–67
Russell, J.M. 1976. ATP-dependent chloride influx into internally dialyzed squid axons. *J. Membrane Biol.* **28**:335–349
Sanders, D. 1980*a*. Control of Cl^- influx in *Chara* by cytoplasmic Cl^- concentration. *J. Membrane Biol.* **52**:51–60
Sanders, D. 1980*b*. The mechanism of Cl^- transport at the plasma membrane of *Chara corallina:* I. Cotransport with H^+. *J. Membrane Biol.* **53**:129–141
Sanders, D., Hansen, U.-P. 1981. Mechanism of Cl^- transport at the plasma membrane of *Chara corallina:* II. Transinhibition and the determination of H^+/Cl^- binding order from a reaction kinetic model. *J. Membrane Biol.* **58**:139–153
Sanders, D., Slayman, C.L. 1982. Control of intracellular pH. Predominant role of oxidative metabolism, not proton transport in the eukaryotic microorganism *Neurospora*. *J. Gen. Physiol.* **80**:377–402
Sanders, D., Slayman, C.L., Hansen, U.-P., Gradmann, D. 1982. Kinetic role of ions in gradient-coupled transport systems. *J. Gen. Physiol.* **80**:22*a*
Schultz, S.G., Curran, P.F. 1970. Coupled transport of sodium and organic solutes. *Physiol. Rev.* **50**:637–718
Schwab, W.G.W., Komor, E. 1978. A possible mechanistic role of the membrane potential in proton-sugar cotransport of *Chlorella*. *FEBS Lett.* **87**:157–160
Schwert, G.W. 1954. Steady-state kinetics of two-substrate enzyme systems. *Fed. Proc.* **13**:293–294
Segel, I.H. 1975. Enzyme Kinetics. Wiley & Sons, New York
Stein, W.D. 1976. An algorithm for writing down flux equations for carrier kinetics, and its application to co-transport. *J. Theor. Biol.* **62**:467–478
Stock, J., Roseman, S. 1971. A sodium-dependent sugar co-transport system in bacteria. *Biochem. Biophys. Res. Commun.* **44**:132–138
Turner, R.J. 1981. Kinetic analysis of a family of cotransport models. *Biochim. Biophys. Acta* **649**:269–280
Turner, R.J., Silverman, M. 1980. Testing carrier models of cotransport using the binding kinetics of non-transported competitive inhibitors. *Biochim. Biophys. Acta* **596**:272–291
Turner, R.J., Silverman, M. 1981. Interaction of phlorizin and sodium with renal brush-border membrane D-glucose transporter: Stoichiometry and order of binding. *J. Membrane Biol.* **58**:43–55
Vidaver, G.A., Shepherd, S.L. 1968. Transport of glycine by hemolysed and restored pigeon red blood cells. *J. Biol. Chem.* **243**:6140–6150
West, I.C. 1980. Energy coupling in secondary active transport. *Biochim. Biophys. Acta* **604**:91–126
Wilbrandt, W., Rosenberg, T. 1961. The concept of carrier transport and its corollaries in pharmacology. *Pharmacol. Rev.* **13**:109–183

Received 14 April 1983; revised 11 July 1983

Appendix I
Derivation of Isotope Flux Equations

The explicit algebraic forms of Eqs. (5) and (6), compressed only by concealment of ligand concentrations and membrane potential, are given in Table A1 for all models implied by the generalized diagram of Fig. 2A. A compact derivation of these relationships, using matrix notation (rather than the more traditional diagrammatic notation [King & Altman, 1956]) to solve for concentrations of individual carrier states, is as follows. The ensemble of steady-state rate equations can be written

$$\mathbf{MV}=\mathbf{N}=N\mathbf{I} \tag{A0}$$

where the matrix (**M**) and vectors (**V**, **N**, and **I**) are defined by

$$\begin{bmatrix} 1 & 1 & 1 & 1 & 1 & 1 \\ -(k_{31}+k_{35}) & k_{13} & 0 & 0 & 0 & k_{53} \\ k_{31} & -(k_{12}+k_{13}) & k_{21} & 0 & 0 & 0 \\ 0 & k_{12} & -(k_{21}+k_{24}) & k_{42} & 0 & 0 \\ 0 & 0 & k_{24} & -(k_{42}+k_{46}) & k_{64} & 0 \\ 0 & 0 & 0 & k_{46} & -(k_{64}+k_{65}) & k_{56} \end{bmatrix} \begin{bmatrix} N_3 \\ N_1 \\ N_2 \\ N_4 \\ N_6 \\ N_5 \end{bmatrix} = \begin{bmatrix} N \\ 0 \\ 0 \\ 0 \\ 0 \\ 0 \end{bmatrix} = N \begin{bmatrix} 1 \\ 0 \\ 0 \\ 0 \\ 0 \\ 0 \end{bmatrix}. \tag{3b}$$

(A1-3) (A1-1) (A1-2) (A1-4) (A1-6)

Table A1. Simplified equations for maximal velocity and Michaelis constant

CONDITIONS	MAXIMAL VELOCITY, J_{max}/N
DOUBLY-LOADED CARRIER POSITIVE (+)	
First-On Models	
Saturating Membrane Potential	$\frac{k_{42}k_{13}k_{35}k_{56}}{k_{42}[(k_{13}+k_{31})(k_{53}+k_{56})+k_{35}(k_{13}+k_{56})]+k_{13}k_{35}k_{56}}$
Zero Trans-Ligand	$\frac{k_{42}k_{21}k_{13}k_{35}k_{56}}{k_{42}[k_{35}k_{56}(k_{21}+k_{12}+k_{13})+k_{21}k_{13}(k_{35}+k_{56})]+k_{35}k_{56}[k_{24}(k_{12}+k_{13})+k_{21}k_{13}]}$
Saturating Cis-Driver Ion	$\frac{k_{21}k_{13}k_{35}k_{56}}{k_{31}(k_{53}+k_{56})(k_{21}+k_{12})+k_{35}k_{56}(k_{21}+k_{12}+k_{13})+k_{21}k_{13}(k_{35}+k_{53}+k_{56})}$
Last-On Models	
Saturating Membrane Potential	$\frac{k_{64}k_{13}k_{35}k_{56}}{k_{64}[(k_{13}+k_{31})(k_{53}+k_{56})+k_{35}(k_{13}+k_{56})]+k_{53}k_{65}(k_{13}+k_{31})+k_{13}k_{35}(k_{56}+k_{65})}$
Zero Trans-Ligand	$\frac{k_{64}k_{21}k_{13}k_{35}k_{56}}{k_{64}[k_{21}k_{13}(k_{35}+k_{56})+k_{35}k_{56}(k_{21}+k_{12}+k_{13})]+k_{21}k_{13}k_{35}(k_{56}+k_{65})}$
Saturating Cis-Driver Ion	
Last-off	$\frac{\{k_{31}k_{24}k_{12}(k_{53}+k_{56})+k_{35}k_{56}[k_{24}(k_{12}+k_{13})+k_{21}k_{13}]\}k_{21}k_{13}k_{35}}{[k_{31}(k_{53}+k_{56})(k_{21}+k_{12})+k_{35}k_{56}(k_{21}+k_{12}+k_{13})+k_{21}k_{13}(k_{35}+k_{53}+k_{56})]\{k_{31}k_{12}k_{24}+k_{35}[k_{24}(k_{12}+k_{13})+k_{21}k_{13}]\}}$
First-off	$\frac{\{k_{53}k_{24}k_{12}k_{31}+k_{56}[k_{13}k_{35}(k_{24}+k_{21})+k_{24}k_{12}(k_{31}+k_{35})]\}k_{21}k_{13}}{\{k_{53}[k_{21}(k_{13}+k_{31})+k_{12}k_{31}]+k_{56}(k_{21}+k_{12})(k_{31}+k_{35})+k_{13}[k_{21}(k_{35}+k_{56})+k_{35}k_{56}]\}\{k_{24}(k_{12}+k_{13})+k_{21}k_{13}\}}$
UNLOADED CARRIER NEGATIVE (-)	
First-On Models	
Saturating Membrane Potential	
Last-off	$\frac{k_{42}k_{21}k_{13}k_{35}}{k_{42}[(k_{21}+k_{12})(k_{31}+k_{35})+k_{13}(k_{21}+k_{35})]+k_{24}k_{12}(k_{31}+k_{35})+k_{13}k_{35}(k_{24}+k_{21})}$
First-off	$\frac{k_{42}k_{21}k_{13}\{k_{42}k_{21}k_{13}k_{35}+k_{46}[k_{24}k_{12}(k_{31}+k_{35})+k_{13}k_{35}(k_{24}+k_{21})]\}}{\{k_{42}[(k_{21}+k_{12})(k_{31}+k_{35})+k_{13}(k_{21}+k_{35})]+k_{24}k_{12}(k_{31}+k_{35})+k_{13}k_{35}(k_{24}+k_{21})\}\{k_{42}k_{21}k_{13}+k_{46}[k_{24}k_{12}+k_{13}(k_{24}+k_{21})]\}}$
Zero Trans-Ligand	$\frac{k_{42}k_{21}k_{13}k_{35}k_{56}}{k_{42}[k_{35}k_{56}(k_{21}+k_{12}+k_{13})+k_{21}k_{13}(k_{35}+k_{53})]+k_{35}[k_{24}(k_{12}k_{56}+k_{13}k_{53})+k_{21}k_{13}k_{56}]}$
Saturating Cis-Driver Ion	$\frac{k_{21}k_{13}k_{35}k_{56}}{k_{31}(k_{21}+k_{12})(k_{53}+k_{56})+k_{21}k_{13}(k_{35}+k_{53}+k_{56})+k_{35}k_{56}(k_{21}+k_{12}+k_{13})}$
Last-On Models	
Saturating Membrane Potential	
Last-off	$\frac{k_{64}k_{21}k_{13}k_{35}}{k_{64}[(k_{21}+k_{12})(k_{31}+k_{35})+k_{13}(k_{21}+k_{35})]+k_{21}k_{13}k_{35}}$
First-off	$\frac{k_{64}k_{21}k_{13}[k_{13}k_{35}(k_{24}+k_{21})+k_{24}k_{12}(k_{31}+k_{35})]}{\{k_{64}[(k_{21}+k_{12})(k_{31}+k_{35})+k_{13}(k_{21}+k_{35})]+k_{21}k_{13}k_{35}\}[k_{24}(k_{12}+k_{13})+k_{21}k_{13}]}$
Zero Trans-Ligand	$\frac{k_{64}k_{21}k_{13}k_{35}k_{56}}{k_{64}[k_{35}k_{56}(k_{21}+k_{12}+k_{13})+k_{21}k_{13}(k_{35}+k_{56})]+k_{21}k_{13}k_{35}(k_{56}+k_{65})}$
Saturating Cis-Driver Ion	
Last-off	$\frac{\{k_{31}k_{24}k_{12}(k_{53}+k_{56})+k_{35}k_{56}[k_{24}(k_{12}+k_{13})+k_{21}k_{13}]\}k_{21}k_{13}k_{35}}{[k_{31}(k_{53}+k_{56})(k_{21}+k_{12})+k_{21}k_{13}(k_{35}+k_{53}+k_{56})+k_{35}k_{56}(k_{21}+k_{12}+k_{13})]\{k_{31}k_{24}k_{12}+k_{35}(k_{24}(k_{12}+k_{13})+k_{21}k_{13}]\}}$
First-off	$\frac{\{(k_{53}+k_{56})k_{24}k_{12}k_{31}+[k_{24}(k_{12}+k_{13})+k_{21}k_{13}]k_{35}k_{56}\}k_{21}k_{13}}{\{(k_{53}+k_{56})[k_{31}(k_{21}+k_{12})+k_{21}k_{13}]+k_{35}[k_{56}(k_{21}+k_{12}+k_{13})+k_{21}k_{13}]\}[k_{24}(k_{12}+k_{13})+k_{21}k_{13}]}$

This table gives the explicit forms of text Eqs. (5) and (6) for three useful simplifications: saturating $\Delta\psi$ (cell interior negative), zero trans-ligand, and saturating cis-driver ion. The upper half table treats only the doubly loaded carrier as charged (+), and the lower half table treats only the unloaded carrier as charged (−). The terms for ion concentration ($[H^+]_o$, $[H^+]_i$) and membrane potential ($\Delta\psi$) have not been extracted; this simplifies the algebraic grouping of terms and in some cases makes the equations identical for first-off and last-off models under each main heading (i.e., "FF"="FL,"

MICHAELIS CONSTANT, K_m	EQUATION NUMBER
$\frac{(k_{42}+k_{46})[k_{53}k_{65}(k_{13}+k_{31}) + k_{13}k_{35}(k_{56}+k_{65})]}{k^o_{64}\{k_{42}[(k_{13}+k_{31})(k_{53}+k_{56}) + k_{35}(k_{13}+k_{56})] + k_{13}k_{35}k_{56}\}}$	A13a,b
$\frac{(k_{42}k_{21}k_{13} + k_{46}[k_{24}(k_{12}+k_{13}) + k_{21}k_{13}]\}\, k_{35}(k_{56}+k_{65})}{k^o_{64}\{k_{42}[k_{35}k_{56}(k_{21}+k_{12}+k_{13}) + k_{21}k_{13}(k_{35}+k_{56})] + k_{35}k_{56}[k_{24}(k_{12}+k_{13}) + k_{21}k_{13}]\}}$	A14a,b
$\frac{k_{31}k_{53}k_{65}(k_{21}+k_{12}) + k_{21}k_{13}[k_{65}(k_{35}+k_{53}) + k_{35}k_{56}]}{k^o_{64}[k_{31}(k_{53}+k_{56})(k_{21}+k_{12}) + k_{35}k_{56}(k_{21}+k_{12}+k_{13}) + k_{21}k_{13}(k_{35}+k_{53}+k_{56})]}$	A15a,b
$\frac{k_{64}k_{13}k_{35}k_{56} + k_{46}[k_{53}k_{65}(k_{13}+k_{31}) + k_{13}k_{35}(k_{56}+k_{65})]}{k^o_{42}\{k_{64}[(k_{13}+k_{31})(k_{53}+k_{56}) + k_{35}(k_{13}+k_{56})] + k_{53}k_{65}(k_{13}+k_{31}) + k_{13}k_{35}(k_{56}+k_{65})\}}$	A16a,b
$\frac{[k_{64}k_{35}k_{56} + k_{46}k_{35}(k_{56}+k_{65})][k_{24}(k_{12}+k_{13}) + k_{21}k_{13}]}{k^o_{42}\{k_{64}[k_{21}k_{13}(k_{35}+k_{56}) + k_{35}k_{56}(k_{21}+k_{12}+k_{13})] + k_{21}k_{13}k_{35}(k_{56}+k_{65})\}}$	A17a,b
$\frac{k_{31}k_{24}k_{12}(k_{53}+k_{56}) + k_{35}k_{56}(k_{24}(k_{12}+k_{13}) + k_{21}k_{13})}{k^o_{42}[k_{31}(k_{53}+k_{56})(k_{21}+k_{12}) + k_{35}k_{56}(k_{21}+k_{12}+k_{13}) + k_{21}k_{13}(k_{35}+k_{53}+k_{56})]}$	A18a,b
$\frac{k_{53}k_{24}k_{12}k_{31} + k_{56}[k_{13}k_{35}(k_{24}+k_{21}) + k_{24}k_{12}(k_{31}+k_{35})]}{k^o_{42}\{k_{53}[k_{21}(k_{13}+k_{31}) + k_{12}k_{31}] + k_{56}(k_{21}+k_{12})(k_{31}+k_{35}) + k_{13}[k_{21}(k_{35}+k_{56}) + k_{35}k_{56}]\}}$	A19a,b
$\frac{k_{42}k_{21}k_{13}k_{35} + k_{46}(k_{24}k_{12}(k_{31}+k_{35}) + k_{13}k_{35}(k_{24}+k_{21}))\}}{k^o_{64}\{k_{42}[(k_{21}+k_{12})(k_{31}+k_{35}) + k_{13}(k_{21}+k_{35})] + k_{24}k_{12}(k_{31}+k_{35}) + k_{13}k_{35}(k_{24}+k_{21})\}}$	A20a,b
Same as for "FL", immediately above	A21a,b
$\frac{k_{42}k_{35}[k_{13}(k_{46}+k_{21})(k_{56}+k_{65}) + k_{12}k_{46}(k_{56}+k_{65})] + k_{46}k_{21}k_{13}k_{35}(k_{56}+k_{65})}{k^o_{64}\{k_{42}[k_{35}k_{56}(k_{21}+k_{12}+k_{13}) + k_{21}k_{13}(k_{35}+k_{53})] + k_{35}[k_{24}(k_{12}k_{56} + k_{13}k_{53}) + k_{21}k_{13}k_{56}]\}}$	A22a,b
$\frac{k_{31}k_{53}k_{65}(k_{21}+k_{12}) + k_{21}k_{13}[k_{65}(k_{35}+k_{53}) + k_{35}k_{56}]}{k^o_{64}\{k_{31}(k_{21}+k_{12})(k_{53}+k_{56}) + k_{21}k_{13}(k_{35}+k_{53}+k_{56}) + k_{35}k_{56}(k_{21}+k_{12}+k_{13})\}}$	A23a,b
$\frac{(k_{64}+k_{46})[k_{13}k_{35}(k_{24}+k_{21}) + k_{24}k_{12}(k_{31}+k_{35})]}{k^o_{42}\{k_{64}[(k_{21}+k_{12})(k_{31}+k_{35}) + k_{13}(k_{21}+k_{35})] + k_{21}k_{13}k_{35}\}}$	A24a,b
Same as for "LL", immediately above.	A25a,b
$\frac{[(k_{64}+k_{46})k_{56} + k_{65}k_{46}][k_{24}(k_{12}+k_{13}) + k_{21}k_{13}]\, k_{35}}{k^o_{42}\{k_{64}[k_{35}k_{56}(k_{21}+k_{12}+k_{13}) + k_{21}k_{13}(k_{35}+k_{56})] + k_{21}k_{13}k_{35}(k_{56}+k_{65})\}}$	A26a,b
$\frac{k_{31}k_{24}k_{12}(k_{53}+k_{56}) + k_{35}k_{56}[k_{24}(k_{12}+k_{13}) + k_{21}k_{13}]}{k^o_{42}[k_{31}(k_{53}+k_{56})(k_{21}+k_{12}) + k_{21}k_{13}(k_{35}+k_{53}+k_{56}) + k_{35}k_{56}(k_{21}+k_{12}+k_{13})]}$	A27a,b
$\frac{(k_{53}+k_{56})k_{24}k_{12}k_{31} + [k_{24}(k_{12}+k_{13}) + k_{21}k_{13}]\, k_{35}k_{56}}{k^o_{42}\{(k_{53}+k_{56})[k_{31}(k_{21}+k_{12}) + k_{21}k_{13}] + k_{35}[k_{56}(k_{21}+k_{12}+k_{13}) + k_{21}k_{13}]\}}$	A28a,b

"LF"="LL"). [The general condition for this equivalence is that the constrained reaction parameter must lie between the reaction steps for binding and release of substrate.] In all cases terms have been grouped so that $[H^+]_o$ (preferably) or $[H^+]_i$ will come out as simple coefficients when the parameter equivalences in the legend to Fig. 2 are substituted. Regrouping of terms and substitution of text Eqs. (1) or (2) are required to obtain convenient expressions with membrane potential. The resultant more elaborate equations are given for one case, "FL," as text Eqs. (7)–(12).

In this form, the first equation represents conservation of total carrier, text Eq. (3b). The other equations are the steady-state expressions specifying that each state of the carrier is generated by two reactions and destroyed (−) by two reactions. One additional equation (i.e., (A1-5): $N_3k_{35}+N_6k_{65}-N_5(k_{53}+k_{56})=0$) is redundant, and has been omitted. The density of each carrier state, N_1 to N_6, can now be written as

$$N_j=N\cdot|\mathbf{M}_j|/|\mathbf{M}| \tag{A2}$$

in which $|\mathbf{M}|$ is the determinant of $\mathbf{M}$ and $|\mathbf{M}_j|$ is the determinant of the matrix obtained by substituting the vector $\mathbf{I}$ for the j-th column in $\mathbf{M}$. As will be seen below, in order to characterize the influx of isotopically labeled substrate (counterclockwise transit in Figs. 1 and 2) only carrier state densities N_6 and N_4 need actually be solved.

It is convenient to group the explicit terms of the denominator differently depending on whether labeled substrate binds in the reaction N_6 to N_4 or the reaction N_4 to N_2. Because the 6-state models of Figs. 1 and 2 are single unbranched loops, each reaction constant appears as a simple factor in 15 terms of the expanded determinant $|\mathbf{M}|$ (36 terms total). Equation (A2) can thus be rewritten, for the two key states, as

$$N_4=N\cdot|\mathbf{M}_4|/(A_4+k_{42}B_4) \tag{A3-4}$$

and

$$N_6=N\cdot|\mathbf{M}_6|/(A_6+k_{64}B_6). \tag{A3-6}$$

It remains only to note (legend to Fig. 2) that, for the models of Fig. 1 *C–D*, $k_{42}=k^o_{42}[S]_o$; and, for the models of Fig. 1 *A–B*, $k_{64}=k^o_{64}[S]_o$. We thus have N, $\mathbf{M}_j$, A_j, k^o, and B_j as used in Eqs. (5) and (6) and Table 1. Analogous calculations by the King and Altman (1956) method generate expressions identical to those in Table 1. Boudart's (1976) method can also be used (*see* Chapman, 1982), though its utility is restricted because the reaction constants subsume concentrations of carrier states which are not known *a priori*.

Terms P and $^*\mathbf{M}$ in Eqs. 5, 6 and Table 1 concern specifically that fraction of the carrier system which is bound to isotope. Provided experiments are executed with zero isotopic labeling of intracellular substrate and with extracellular isotope added at zero time (usual arrangement for initial rate measurements), then passage of chemical substrate (S) from inside to outside (clockwise in Figs. 1 and 2) will not falsify the isotope flux *per se*. It will, however, perturb the isotope influx by dilution of carrier. This means that the simple dissociation reactions $SXH^+ \rightleftharpoons XH^+ + S_i$ or $SX \rightleftharpoons X + S_i$ cannot gauge the isotope flux because the specific activity of S bound to those "unloading" states of the carrier is less than the specific activity of S in the external solution. In other words, if the transport reaction is expressed in the conventional format of enzyme kinetics ($X+S\rightarrow X+P$; Page & West, 1981), an estimate of the isotopic flux will only result if $P=0$, or if it is explicitly recognized that P is chemically identical to S. The traditional method of solving this problem is to calculate backwards from the "unloading" state to the "loading" state of the carrier (e.g., Cleland, 1967; Cuppoletti & Segel, 1975*b*), at which point the relevant specific activity is just that of the external medium, $[^*S]_o/[S]_o$.

The method is most simply illustrated for the last on-first off model (Fig. 1*D*). Again using the steady-state assumption,

$$d^*N_1/dt=0=-{}^*N_1(k_{12}+k_{13})+{}^*N_2k_{21} \tag{A4-1}$$

in which * designates isotopically tagged carrier. The N_3 term is missing because no isotope is present inside the cell. The next step backwards is

$$d^*N_2/dt=0={}^*N_1k_{12}-{}^*N_2(k_{21}+k_{24})+N_4[^*S_o]k^o_{42}. \tag{A4-2}$$

No further steps are necessary, since both $^*N_1$ and $^*N_2$ can now be solved in terms of the unlabeled carrier state N_4 and isotopically labeled extracellular substrate *S.

The two Eqs. (A4-1, 2) can be rewritten in matrix form as

$$\begin{bmatrix}-(k_{12}+k_{13}) & k_{21}\\ k_{12} & -(k_{21}+k_{24})\end{bmatrix}\begin{bmatrix}{}^*N_1\\ {}^*N_2\end{bmatrix}$$
$$=\begin{bmatrix}0\\ -N_4[^*S]_ok^o_{42}\end{bmatrix}=N_4[^*S]_ok^o_{42}\begin{bmatrix}0\\ -1\end{bmatrix} \tag{A5}$$

which is related to Eq. (A1) above by the fact that the left-hand matrix in (A5) is a submatrix of the left-hand matrix in (A1). And the corresponding isotope equations for the other three models (Figs. 1*A–C*) can be written down almost directly from Eq. (A1) by lengthening the matrix diagonal of Eq. (A5) to include the term $-(k_{31}+k_{35})$ for the last-off models and include $-(k_{42}+k_{46})$ for the first-on models.

Thus, the first on-first off model (Fig. 1*B*) gives

$$\begin{bmatrix}-(k_{12}+k_{13}) & k_{21} & 0\\ k_{12} & -(k_{21}+k_{24}) & k_{42}\\ 0 & k_{24} & -(k_{42}+k_{46})\end{bmatrix}\begin{bmatrix}{}^*N_1\\ {}^*N_2\\ {}^*N_4\end{bmatrix}$$
$$=N_6[^*S]_ok^o_{64}\begin{bmatrix}0\\ 0\\ -1\end{bmatrix}; \tag{A6}$$

the last on-last off model (Fig. 1*C*) gives

$$\begin{bmatrix}-(k_{31}+k_{35}) & k_{13} & 0\\ k_{31} & -(k_{12}+k_{13}) & k_{21}\\ 0 & k_{12} & -(k_{21}+k_{24})\end{bmatrix}\begin{bmatrix}{}^*N_3\\ {}^*N_1\\ {}^*N_2\end{bmatrix}$$
$$=N_4[^*S]_ok^o_{42}\begin{bmatrix}0\\ 0\\ -1\end{bmatrix}; \tag{A7}$$

and finally, the first on-last off model (Fig. 1*A*) gives

$$\begin{bmatrix}-(k_{31}+k_{35}) & k_{13} & 0 & 0\\ k_{31} & -(k_{12}+k_{13}) & k_{21} & 0\\ 0 & k_{12} & -(k_{21}+k_{24}) & k_{42}\\ 0 & 0 & k_{24} & -(k_{42}+k_{46})\end{bmatrix}$$
$$\begin{bmatrix}{}^*N_3\\ {}^*N_1\\ {}^*N_2\\ {}^*N_4\end{bmatrix}=N_6[^*S]_ok^o_{64}\begin{bmatrix}0\\ 0\\ 0\\ -1\end{bmatrix}. \tag{A8}$$

All four of these equations may then be solved for the "unloading" state of the isotopically labeled carrier ($^*N_3$ in the last-off models; $^*N_1$ in the first-off models) in terms of the external concentration of labeled substrate ($[^*S]_o$) and the "loading" state of the carrier (N_6 for the first-on models; and N_4 for the last-on models). Solution by determinants is exactly analogous to Eq. (A2), and can be written as

$$^*N_i=N_4[^*S]_ok^o_{42}\cdot|^*\mathbf{M}_i|/|^*\mathbf{M}| \tag{A9a}$$

or

$$^*N_i = N_6[^*S]_o k^o_{64} \cdot |^*\mathbf{M}_i|/|^*\mathbf{M}| \quad \text{(A9b)}$$

in which the subscript i has the value 1 or 3 and $|^*\mathbf{M}|$ is the determinant for the left-hand matrix in Eqs. (A5), (A6), (A7), or (A8) and indicated in text Eqs. (5) and (6) and Table 1. The unidirectional isotope influx (counterclockwise in Figs. 1 and 2) is then given by the product of $^*N_i$ and the appropriate dissociation constant:

$$^*J_S = {}^*N_1 k_{13} \quad \text{or} \quad {}^*J_S = {}^*N_3 k_{35} \quad \text{(A10-1, 3)}$$

which corresponds to text Eq. (4). Since there are two values for $^*N_1$ and two for $^*N_3$, combination of Eqs. (A10-1, 3) with Eqs. (A3-4, 6) gives four flux equations in all, one for each diagram in Fig. 1. Partial algebraic expansion of each equation yields the following kind of result (e.g., for the first on-last off model, Fig. 1*A*):

$$^*J_S = N \frac{|\mathbf{M}_6|}{|^*\mathbf{M}|} \frac{k_{42}k_{21}k_{13}k_{35}k^o_{64}[^*S]_o}{A_6 + B_6 k^o_{64}[^*S]_o}. \quad \text{(A11a)}$$

Upon division of numerator and denominator by $B_6 k^o_{64}$, k^o_{64} cancels out of the numerator, so that the product of clockwise reaction constants is simply

$$P \equiv k_{42}k_{21}k_{13}k_{35}. \quad \text{(A12a)}$$

Equations similar to Eqs. (A11a) and (A12a) can be written for all three other cotransport diagrams in Fig. 1. The full expansions of terms, in all four binding and unloading sequences, are listed in Table 1. Equation (A11a) and its congeners have the overall form of a Michaelis-Menten relationship, for which K_m and J_{max} are given in text Eqs. (5) and (6). Since all extracellular substrate is isotopically labeled (after zero time in an initial-rate experiment) at a fixed specific activity, we have omitted the label notation * from text Eqs. (4)–(6) and from Table 1.

Appendix II
Reserve Factors and the Effects of Concealed Carrier States

Throughout the discussion above, it was convenient to assume that the model represented by Fig. 2*A*, Eqs. (4)–(6), and the matrix relations of Eqs. (A0), (A1), and (A5)–(A9) is realistic and accurate with respect to the number and arrangement of functional carrier states. In general, this is unlikely to be true for complex reactions, and models like those of Figs. 1 and 2 should properly be regarded as *pseudo* 6-state models that approximate *real* n-state systems.

The question naturally arises, therefore, of how the presence of unidentified carrier states in a real system for cotransport would affect the kinetic relationships outlined above. The purpose of this Appendix is to show that *unidentified states have no qualitative effect* on the kinetic behavior of cotransport systems, at least if the flux measurements are made with the transport system in steady state [$dN_i/dt = 0$; *see* assumption (ii), near Eq. (3a)]. We shall use the general approach adopted for the description of current-voltage relationships (Hansen et al., 1981; pp. 169 & 186–187), and define (i) a set of *reserve* factors – designated $r_i (i = 1, 2, \ldots, 6)$ – which formally accommodate the concealed carrier states, and (ii) a set of *empirical* reaction constants – designated κ_{12}, κ_{24}, etc. – which would actually be computed by analyzing experimental data without inclusion of the reserve factors.

[Previous analyses of the behavior of reduced transport- or enzyme-kinetic models have been given by several authors, including Cha (1968), Hill (1977), and Reich and Sel'kov (1981). In all those cases, however, the key to model reduction was to assume equilibrium for certain segments of the particular reaction diagram. Although it eliminates reserve factors and selected reaction constants, that procedure is akin to the *a priori* assumption of rate limitation by transmembrane transfer, and is not satisfactory in the present context.]

Physical Significance of Reserve Factors

Suppose a particular reaction step, say $N_6 \rightleftharpoons N_5$ in Fig. 2*A*, actually contains one unidentified carrier state (z), so that $N_6 \rightleftharpoons N_z \rightleftharpoons N_5$. Obviously, on analysis by a 6-state model, state z will appear added partially to state 6 and partially to state 5. In fact, N_z can be written as a relatively simple algebraic function of its associated reaction constants (Hansen et al., 1981; Gradmann et al., 1982):

$$N_z = \frac{k_{5z}}{k_{z5} + k_{z6}} N_5 + \frac{k_{6z}}{k_{z5} + k_{z6}} N_6 = r_{5z} N_5 + r_{6z} N_6 \quad \text{(A29)}$$

in which the right-hand terms serve to define partial reserve factors. If other reaction steps adjacent to $N_6 \rightleftharpoons N_5$ also contain concealed carriers, or if the transition between states 6 and 5 is still more complicated, then all contributing terms must be included in the total reserve factors, so that

$$r_5 = 1 + r_{5z} + r_{5x} + \ldots \quad \text{and} \quad r_6 = 1 + r_{6z} + r_{6y} + \ldots \quad \text{(A30)}$$

where the subscripts x and y denote additional concealed carrier states. The summary relationships between the *apparent* density of carrier state 5 ($\bar{N}_5$) or carrier state 6 ($\bar{N}_6$) and the respective *real* densities (N_5, N_6) are then

$$\bar{N}_5 = r_5 N_5 \quad \text{and} \quad \bar{N}_6 = r_6 N_6 \quad \text{(A31a, b)}$$

or more generally

$$\bar{N}_i = r_i N_i \quad \text{and} \quad \bar{N}_j = r_j N_j \quad \text{(A31c, d)}$$

when the possible presence of unknown carrier states in all steps of Fig. 2 is allowed.

Evidently, kinetic analysis carried out without knowledge of the composite nature of the $N_5 \rightleftharpoons N_6$ transition would find reaction velocities (J_{56}, J_{65}) to be the product of each apparent state density times an apparent or *empirical* reaction constant:

$$J_{56} = \bar{N}_5 \kappa_{56}, \quad J_{65} = \bar{N}_6 \kappa_{65}. \quad \text{(A32)}$$

On the other hand, if we imagine an alternative reaction scheme in which $N_6 \rightleftharpoons N_5$ does take place without concealed states and at the *same velocity* as in $N_6 \rightleftharpoons N_z \rightleftharpoons N_5$, then

$$J_{56} = N_5 k_{56} \quad \text{and} \quad J_{65} = N_6 k_{65} \quad \text{(A33)}$$

whence it follows that (in general form)

$$\kappa_{ij} = k_{ij}/r_i \quad \text{and} \quad \kappa_{ji} = k_{ji}/r_j. \quad \text{(A34)}$$

Equations (A31)–(A34) are a formal statement of an important and intuitively evident circumstance: that the observed reaction rate between two carrier states (i.e., the reaction product $N_i k_{ij}$) is not affected by the presence of unidentified carrier states. This means that *distortion in*

kinetic analysis arises only in the manner of partitioning the rate product between the carrier state density and the reaction rate constant.

The Pseudo 6-State Model

With the model of Fig. 2*A* taken as a pseudo model, so that the real system contains unidentified carrier states, carrier conservation must be represented by Eq. (3a), rather than (3b), and Eq. (A1) becomes

$$\begin{bmatrix} r_3 & r_1 & r_2 & r_4 & r_6 & r_5 \\ -(k_{31}+k_{35}) & k_{13} & 0 & 0 & 0 & k_{53} \\ k_{31} & -(k_{12}+k_{13}) & k_{21} & 0 & 0 & 0 \\ 0 & k_{12} & -(k_{21}+k_{24}) & k_{42} & 0 & 0 \\ 0 & 0 & k_{24} & -(k_{42}+k_{46}) & k_{64} & 0 \\ 0 & 0 & 0 & k_{46} & -(k_{64}+k_{65}) & k_{56} \end{bmatrix} \begin{bmatrix} N_3 \\ N_1 \\ N_2 \\ N_4 \\ N_6 \\ N_5 \end{bmatrix} = N \begin{bmatrix} 1 \\ 0 \\ 0 \\ 0 \\ 0 \\ 0 \end{bmatrix}. \tag{A35}$$

By means of Eqs. (A31c, d) and (A34), the above matrix can be converted back to the *form* of (A1), *viz.*,

$$\begin{bmatrix} 1 & 1 & 1 & 1 & 1 & 1 \\ -(\kappa_{31}+\kappa_{35}) & \kappa_{13} & 0 & 0 & 0 & \kappa_{53} \\ \kappa_{31} & -(\kappa_{12}+\kappa_{13}) & \kappa_{21} & 0 & 0 & 0 \\ 0 & \kappa_{12} & -(\kappa_{21}+\kappa_{24}) & \kappa_{42} & 0 & 0 \\ 0 & 0 & \kappa_{24} & -(\kappa_{42}+\kappa_{46}) & \kappa_{64} & 0 \\ 0 & 0 & 0 & \kappa_{46} & -(\kappa_{64}+\kappa_{65}) & \kappa_{56} \end{bmatrix} \begin{bmatrix} \bar{N}_3 \\ \bar{N}_1 \\ \bar{N}_2 \\ \bar{N}_4 \\ \bar{N}_6 \\ \bar{N}_5 \end{bmatrix} = N \begin{bmatrix} 1 \\ 0 \\ 0 \\ 0 \\ 0 \\ 0 \end{bmatrix}. \tag{A36}$$

Equations (A31), (A34), and (A36) can be generalized to the representation of any real n-state system by that m-state model ($m<n$) which is most convenient in relation to a particular ensemble of experiments.

Practical Consequences

The essential practical consequence of Eq. (A36) and its congeners is that no generality is lost by reduced kinetic representation of a complex system, provided that incorporation of reserve factors into the empirical reaction constants is kept in mind. Since, for steady-state systems, each reserve factor is a definite algebraic function of involved real reaction constants, subsequent knowledge of intermediate states makes possible exact calculation of the N_i's and k_{ij}'s, given knowledge of the $\bar{N}_i$'s and κ_{ij}'s from a particular model. Thus, *with appropriate bookkeeping via reserve factors,* reduced models for a reaction system yield families of apparent state densities and reaction constants which can be converted to physically more realistic families as further data emerge. In practical analysis of transport kinetics, relevant further data can be expected from new techniques: spectrophotometric tracing of individual carrier states, double isotope flux analysis, use of site-specific inhibitors, or activation by substrate analogues, to suggest a few.

A simple example serves to illustrate the practical consequences of concealed carrier states. In the reaction chain $N_6 \rightleftharpoons N_z \rightleftharpoons N_5$ containing the concealed state z, let the density of the three states be 100 and the magnitudes of all reaction constants equal 1,000; the reserve factor r_6 will assume the value 1.5 [Eqs. (A29) and (A30)]. Hence the empirical rate constant κ_{65} will be 667 [Eq. (A34)], instead of 1,000; and correspondingly, the apparent carrier density in state 6 ($\bar{N}_6$) will be 150 [Eq. (A31b)], rather than 100. Thus, the measured and real rates of unidirectional decay for carrier state 6 coincide ($\bar{N}_6\kappa_{65} = N_6 k_{6z} = 10^5$). From an experimental point of view, of course, the distortion will always appear in κ_{65}, because only the total carrier density (N), for all states, appears in the resolved kinetic equations.

One note of caution, however, is in order. In the partial reaction $N_4 \rightleftharpoons N_6 \rightleftharpoons N_z \rightleftharpoons N_5 \rightleftharpoons N_3$, the presence of (unknown) state z distorts not only reaction constants κ_{56} and κ_{65}, but also k_{53} and k_{64} (which must be written as κ_{53} and κ_{64}). This happens because the steady-state velocities J_{53} and J_{64} contain *apparent* state densities $\bar{N}_6$ and $\bar{N}_5$. We have previously classified such *transfer* effects as either parallel-positive or antiparallel negative - depending on the particular choice of reaction constants, for a pseudo 2-state representation of ion pumping, in which the primary experimental variable was membrane potential (Hansen et al., 1981). Similar classification is possible for larger kinetic models and variable ligand concentrations.